

Probing the possibility of coexistence of martensite transition and half-metallicity in Ni and Co-based full Heusler Alloys : An ab initio Calculation

Tufan Roy¹, Dhanshree Pandey¹ and Aparna Chakrabarti^{1,2}

¹*HBNI, Raja Ramanna Centre for Advanced Technology, Indore - 452013, India and*

²*ISUD, Raja Ramanna Centre for Advanced Technology, Indore - 452013, India*

Using first-principles calculations based on density functional theory, we have studied the mechanical, electronic, and magnetic properties of Heusler alloys, namely, Ni_2BC and Co_2BC ($B = \text{Sc, Ti, V, Cr}$ and Mn as well as Y, Zr, Nb, Mo and Tc ; $C = \text{Ga}$ and Sn). On the basis of electronic structure (density of states) and mechanical properties (tetragonal shear constant), as well as magnetic interactions (Heisenberg exchange coupling parameters), we probe the properties of these materials in detail. We calculate the formation energy of these alloys in the (face-centered) cubic austenite structure to probe the stability of all these materials. From the energetic point of view, we have studied the possibility of the electronically stable alloys having a tetragonal phase lower in energy compared to the respective cubic phase. A large number of the magnetic alloys is found to have the cubic phase as their ground state. On the other hand, for another class of alloys, the tetragonal phase has been found to have lower energy compared to the cubic phase. Further, we find that the values of tetragonal shear constant show a consistent trend : a high positive value for materials not prone to tetragonal transition and low or negative for others. In the literature, materials, which have been seen to undergo the martensite transition, are found to be metallic in nature. We probe here if there is any Heusler alloy which has a tendency to undergo a tetragonal transition and at the same time possesses a high spin polarization at the Fermi level. From our study, it is found that out of the four materials, which exhibit a martensite phase as their ground state, three of these, namely, Ni_2MnGa , Ni_2MoGa and Co_2NbSn have a metallic nature; on the contrary, Co_2MoGa exhibits a high spin polarization.

PACS numbers: 71.20.Be, 71.15.Nc, 71.15.Mb, 81.30.Kf, 75.50.Cc

I. INTRODUCTION

Heusler alloys are intermetallic compounds with interesting fundamental properties and possible practical applications. Heusler alloys are typically known to be of two types: full-Heusler alloys (FHA) and half-Heusler alloys (HHA). The full-Heusler alloys, which are having a formula A_2BC (with a stoichiometry 2:1:1, e.g. Ni_2MnGa), commonly exhibit a $L2_1$ structure. This has four interpenetrating face-centered (fcc) sub-lattices, for each of the atoms $A(\text{Ni})$, $A(\text{Ni})$, $B(\text{Mn})$ and $C(\text{Ga})$. On the other hand, the half-Heusler alloys with a formula ABC (with a stoichiometry 1:1:1, e.g. NiMnSb) typically assume a $C1_b$ structure where one of the four fcc sub-lattices remains unoccupied. Since the discovery of the prototype FHA, Ni_2MnGa ¹, various studies have been carried out which show that this alloy, having long-range ferromagnetic interaction, possesses various interesting physical properties. For example, Ni_2MnGa exhibits magnetic field induced strain (MFIS) and magnetic shape memory alloy (MSMA) property²⁻⁴, magnetoresistance effect (MRE)⁵ as well as magnetocaloric effect (MCE)⁶.

The Heusler alloys are interesting from both the points of view of possible technological application as well as fundamental science. Hence, these have been enjoying the attention of the researchers - theoreticians and experimentalists alike. Further, the basic drawbacks of the prototype Heusler alloy, Ni_2MnGa , in terms of technological application are its brittleness and the low martensite transition temperature. Therefore, following the discovery of and studies on Ni_2MnGa , various FHAs have been synthesized, characterized and studied in the last two decades, as is observed in the literature. Many new FHA materials, till date, have been predicted from ab initio calculations as well. It has been observed that the face-centered-cubic phase is the high-temperature or the so-called austenite phase of these materials. Some of these FHAs has been seen to undergo a tetragonal distortion at a lower temperature. This first-order displacive transition, generally known as martensite transition, where the volumes of the unit cell of both the austenite and martensite phases are close to each other, is typically connected to the SMA property exhibited by these alloys. Among the FHAs, in terms of the electronic structure, there are various categories. While some of these alloys prefer to be metallic, some are found to be semiconducting, and some are having a large spin-polarization at the Fermi level.^{1,7-9}

If the FHAs are magnetic in nature, their properties can change when a magnetic field is applied which can be of interest in terms of potential technological application. Hence, specially, magnetic shape memory alloys are gaining increasing interest. Therefore, detailed studies of magnetic configurations, properties and interactions are of particular importance. In literature, various magnetic ground state configurations are observed in case of full-Heusler alloys. While some alloys are even non-magnetic, many of these exhibit a long-range ferromagnetic ordering and are expected

to show MSMA property. In many of these MSMA, there is presence of a delocalized-like common d-band formed by the d-electrons of the A and B atoms, which are both typically first-row transition metal atoms.¹⁰ Additionally, there is also an indirect RKKY-type exchange mechanism¹¹, primarily mediated by the electrons of the C atoms, which plays an important role in defining the magnetic properties of these materials.^{1,10,12–14} Further, it has also been observed that some of these alloys including Mn_2NiGa even show long-range ferrimagnetism and also anti-ferromagnetism.^{15–19}

Hence, it is clear from the literature, that in terms of different physical, including, structural (mechanical), electronic and magnetic properties, the full-Heusler alloys show a rich variety. Further, as has been mentioned above, it has been of particular interest that out of all the full-Heusler alloys, only a few undergo the martensite transition. These alloys are prone to a cubic to tetragonal distortion when temperature is lowered and generally exhibit the technologically important SMA property. These FHAs in general are found to be metallic in nature. On the other hand, it has been observed that there is another group of full-Heusler alloys which are half-metallic-like in nature, with a much reduced density of states (DOS) at the Fermi level in case of one of the spin channels. These materials generally do not show the tendency of undergoing a tetragonal distortion and also showing the SMA property. However, an application in the field of spintronics is a possibility for these materials. From both the points of view of fundamental understanding as well as technological application, it can be interesting to probe the similarities and differences in magnetic, bulk mechanical, and electronic properties of these two categories of materials. It will also be interesting to see if there is any FHA which has a tendency to undergo a tetragonal transition and at the same time possesses a high spin polarization at the Fermi level.

Keeping this in mind, in the present paper, we probe the magnetic, bulk mechanical, and electronic properties of a series of Ni and Co-based full Heusler alloys using density functional theory (DFT) based ab initio calculations. The choice of these two systems (Ni and Co-based FHAs) is due to the following facts. First and foremost, it has been seen that typically, a large amount of work on the FHAs are on Ni and Co-based compounds. It is also seen in the literature that while most of the Ni-based FHAs show MSMA property, many of the Co-based FHAs exhibit large spin-polarization at the Fermi level. It has also been pointed out in the literature, that while the magnetic interactions are somewhat different in the Ni and Co-based FHAs, the total energy variation for an austenite to martensite phase transition is similar.²⁰ Hence, a comparative study may be interesting and also important for detailed understanding of the properties of these alloys. The primary interest is to study the possibility of the tetragonal transition versus a high spin polarization at the Fermi level. Further, we look for ferromagnetic materials so that realization of MSMA property is possible. In what follows, first, we give a brief account of the methods we used and then we present the results and discussion. In the end, the results of this work are summarized and conclusions are drawn.

II. METHOD

The full-Heusler alloys, as for example, Ni_2MnGa , commonly assume an ordered A_2BC structure, where typically A , B are elements with d-electrons and C are elements with s,p electrons. In the cubic high-temperature austenite phase, Ni_2MnGa has a $L2_1$ structure that consists of four interpenetrating face-centered-cubic (fcc) sub-lattices with origin at fractional positions, $(0.25, 0.25, 0.25)$, $(0.75, 0.75, 0.75)$, $(0.5, 0.5, 0.5)$, and $(0.0, 0.0, 0.0)$. In $L2_1$ structure of Ni_2MnGa , the Ni atoms occupy the first and second sub-lattices. On the contrary, Mn and Ga occupy the third and fourth sub-lattices, respectively. In this paper, we have carried out calculations on Ni and Co-based systems. So Ni and Co are taken as A atom and $C = Ga$ as well as Sn. As for the B atom, we have taken into consideration and consequently tested the electronic stability of the first five atoms of the first as well as second rows of the transition metal atoms. Therefore, Sc, Ti, V, Cr and Mn as well as Y, Zr, Nb, Mo and Tc are considered as the B atom.

The equilibrium lattice constants of all these alloys are obtained by full geometry optimization using Vienna Ab Initio Simulation Package (VASP)²¹ which has been used in combination with the projector augmented wave (PAW) method²² and the generalized gradient approximation (GGA) over the local density approximation (LDA) for the exchange-correlation functional.²³ GGA is used because it accounts for the density gradients, and hence, for most of the Heusler alloy systems, it has been found that it yields results which are in better agreement with experimental data compared to the results of LDA. We have used an energy cutoff of 500 eV for the planewaves. The final energies have been calculated with a k mesh of $15 \times 15 \times 15$ for the cubic case and a similar number for the tetragonal case. The energy and the force tolerance for our calculations were $10 \mu\text{eV}$ and $10 \text{ meV}/\text{\AA}$, respectively. The formation energies (E_{form}), as calculated²¹ by the equation below, has been critically analysed to establish the electronic stability of the alloys.

$$E_{form} = E_{tot} - \sum_i c_i E_i \quad (1)$$

where i denotes different types of atoms present in the unit cell of the material system and E_i are the standard state energies of the corresponding atoms i .²¹ The optimized geometries of the systems studied are compared with the

results obtained in the literature, wherever results are available, and these match well with earlier data as discussed in the section on Results and Discussion.

The response of a material to an applied stress is associated with the elastic constants of the material. Both stress (σ) and strain (ϵ) in a material have three tensile as well as three shear components. Therefore, the linear elastic constants form a 6×6 symmetric matrix. We have $\sigma_i = C_{ij} \epsilon_j$ for small stresses, σ , and strains, ϵ . Calculations of the mechanical properties of the materials involve the variation of total energy of the system induced by the strain.²¹ Elastic constants of all the materials are evaluated from the second derivative of the energy with respect to the strain tensor. The number of k -points and the energy cut-off have been increased from the values used in SCF calculations till the convergence of the mechanical properties of each individual material has been achieved. Mesh of k -points has been taken as $15 \times 15 \times 15$ and energy cut-off of 500 eV as per the convergence requirement.

It is well known that, all-electron calculations are more reliable for the prediction of magnetic properties particularly for the systems containing first row transition elements. Hence, to calculate and understand in detail the magnetic as well as electronic properties, we have carried out relativistic spin-polarized all-electron calculations of all the systems, geometries being optimized by VASP.²¹ These calculations have been performed using full potential linearized augmented plane wave (FP-LAPW) program²⁴ with the generalized gradient approximation (GGA) for the exchange-correlation functional.²³ For obtaining the electronic properties, the Brillouin zone (BZ) integration has been carried out using the tetrahedron method with Blöchl corrections.²⁴ An energy cut-off for the plane wave expansion of about 17 Ry is used ($R_{MT}K_{max} = 9.5$). The cut-off for charge density is $G_{max} = 14$. The number of k points for the self-consistent field (SCF) cycles in the reducible (irreducible) BZ is about 8000 (256) for the cubic phase and about 8000 (635) for the tetragonal phase. The convergence criterion for the total energy E_{tot} is about 0.1 mRy per atom. The charge convergence is set to 0.0001.

To gain further insight into the magnetic interactions of some of the magnetic materials, we calculate and discuss their Heisenberg exchange coupling parameters. The geometries optimized by VASP have been used for these calculations. We use the Spin-polarized-relativistic Korringa-Kohn-Rostoker method (SPR-KKR) to calculate the Heisenberg exchange coupling parameters, J_{ij} , within a real-space approach, which is proposed by Liechtenstein et al²⁵ and implemented in the SPR-KKR programme package.²⁶ The mesh of k points for the SCF cycles has been taken as $21 \times 21 \times 21$ in the BZ. The angular momentum expansion for each atom is taken such that $l_{max} = 3$. In addition, in terms of the Heisenberg exchange coupling parameters we derive the Curie temperature (T_C) following the literature²⁷.

III. RESULTS AND DISCUSSION

A. Geometry Optimization and Electronic Stability

Lattice parameter and Atomic number Z of B atom - For the cubic phase, the $L2_1$ structure has been assumed for all the structures studied here, namely, Ni_2BC and Co_2BC ($B = Sc, Ti, V, Cr$ and Mn as well as Y, Zr, Nb, Mo and Tc ; $C = Ga$ and Sn). The geometry has been optimized to obtain the converged lattice parameter. Figure 1 and Figure 2 show the variation of this lattice parameter as a function of Z of B elements of A_2BC alloy ($A = Ni, Co$; $C = Ga, Sn$). The B atoms correspond to the period IV of the periodic table (first row transition metal atoms; Sc etc) and the period V (second row transition metal atoms; Y etc). Therefore, in Figures 1 and 2, we have mentioned the period numbers IV and V in the legends. For the Ni_2BC materials, it is observed, as the atomic number of B elements increases, with a saturating trend towards higher Z , lattice parameters of the materials decrease for a fixed row of the periodic table (Figure 1). This may happen due to the increasing electro-negativity and decreasing atomic radius of atoms across the column. Further, for these materials we observe (in the left panel of Figure 1) a sudden increase in the lattice parameter value for Z of $B = 24$ (i.e. Cr atom). It is to be noted that out of all the materials studied here, a deviation from the ferromagnetic nature is expected for Ni_2CrSn as well as Ni_2CrGa which was reported earlier.¹⁹ These two materials have lower energy for a long-range *intra-sublattice* anti-ferromagnetic (AFM) ordering compared to the ferromagnetic (FM) one. This difference in the long-range magnetic interaction between the FHAs with $B = Cr$ and the other B atoms indicates that the Cr -based materials are possibly of a different class compared to the rest of the FHAs, considered here. This may be the reason behind the deviation from the observed trend. It is to be further noted that for the AFM ordering the lattice parameter (shown by a black square) is even larger compared to the corresponding FM phase. However, the long-range magnetic interaction in all the materials with $A = Co$ is ferromagnetic. For these Co -based materials the lattice parameters show a smooth decrease as we increase the Z of the B atom (Figure 2). As discussed above for Ni -based systems, this may, again, be due to the increase of electronegativity and decrease of atomic radius across the column which may have led to the shrinkage of the electron cloud around the B atom, and consequently, of the whole unit cell. It has been observed that there is an increase in the lattice parameter values when we go from period IV to period V, for both Ni and Co -based

materials. Increase of atomic radius is observed across the row, going from period IV to V, and the above-mentioned trend may be because of that.

Formation energy and Atomic number Z of B atom - Figure 3 as well as Figure 4 suggest that the formation energy is negative for all of the materials with C atom = Ga, except Ni_2TcGa which is having marginally positive formation energy. It is to be noted that Co_2TcGa has marginally negative formation energy and hence in reality may not be stable electronically. It is well-known that negative formation energy signifies stability; more negativity indicates more stability of the material. A few of the materials, A_2BC , where $C = \text{Sn}$, like Ni_2MoSn , Ni_2TcSn , Co_2CrSn , Co_2MoSn and Co_2TcSn , are having positive formation energy. These calculated values and the prediction that these particular materials are electronically unstable, matches with the results wherever available in the literature.²⁸ The AFM phases for Ni_2CrGa and Ni_2CrSn have very close but slightly smaller E_{form} compared to the respective FM case. It is observed from both the figures that, overall, there is a trend of electronic stability decreasing as Z of B atom increases. However, for $B = \text{Mn}$, the stability has increased compared to the previous B element. This suggests an interesting preference for the Mn atom in the B position for the Heusler alloys with $L2_1$ structure in both the cases when A atom is Ni or Co. Similar is the case with $B = \text{Zr}$. It is seen that, for Y, i.e. the first atom of the second row of the transition metal atoms (period V) at the B position, the formation energy is somewhat unfavorable compared to the next case of $B = \text{Zr}$. The origin of this has been found to be electronic in nature - analysis of the density of states for $B = \text{Zr}$ indicates a lowering of binding energy in this material compared to the $B = \text{Y}$ case. It is observed that the contribution from the majority spin density of states of the Co atom plays an important role. For our further studies, we concentrate only on the materials which, from our calculations, are found to be electronically stable.

Electronic Stability of the Tetragonal phase - We calculate the difference between the energy of the cubic (E_C) and tetragonal (E_T) phases of all the electronically stable materials. Figure 5 shows this energy difference, $\Delta E = E_T - E_C$ (in units of meV per atom), of some typical materials as a function of the ratio of lattice constants c and a . From our calculations, we find that only a few materials, among all the electronically stable and magnetic FHAs we study here, exhibits the tetragonal phase as a lower energy state. Among all the Ni-based alloys, we find that Ni_2MoGa and Ni_2CrSn possess a lower energy for the tetragonal phase over the cubic phase similar to Ni_2MnGa and Ni_2CrGa , both of which have a tetragonal ground state, as has already been shown in the literature. From Figure 5, we also observe that Ni_2VGa and Ni_2VSn have very flat energy curves with no clear minimum in the ΔE versus c/a curve. Further, we observe that though in case of Ni_2MnSn , there is a cubic ground state, there is also a very subtle signature of a tetragonal phase which is evident from the clear asymmetric nature of the ΔE versus c/a curve for this material (Figure 5). It is observed that Ni_2MoGa exhibits a non-magnetic state as ground state. Further, Ni_2CrGa and Ni_2CrSn are likely to possess an *intra-sublattice* AFM phase as a ground state. It is to be noted that, in this paper, our concentration will be only on the alloys which will have FM phase in its ground state. So, for Ni-based alloys, further on, we will discuss only about Ni_2MnGa and Ni_2MnSn .

Out of all the Co-based alloys studied here, we observe that only two alloys are likely to show energetically lower martensite phase over the cubic austenite phase. Out of these two, while Co_2NbSn is known in the literature²⁹, Co_2MoGa is not reported till date. From Figure 5, it is clearly seen that for Co_2MoGa a significant energy difference exists between the cubic and tetragonal phases. This indicates that a martensite phase transition is possible in this material. It is expected that the martensite transition temperature for Co_2MoGa will be higher than Ni_2MnGa since the energy difference ΔE between the austenite and martensite phase of the former is evidently much larger than that of the latter. This expectation is because it is argued in the literature, that, relative values of ΔE can be indicative of the relative values of martensite transition temperatures of two alloys.^{20,30} A cubic ground state is observed for many Co-based alloys, including the two well-known Co-based half-metallic-like materials Co_2MnSn ³¹ and Co_2MnGa ³². It is interesting to note that there are three more alloys which show a state of cubic symmetry having a lowest energy while the tetragonal phases of these materials are energetically very close (within 25 meV) to the respective austenite phases. The ΔE versus c/a plots of these materials, namely, Co_2VGa , Co_2CrGa and Co_2TcGa are included in Figure 5 which clearly depict this energetic aspect.

In Table 1 we report the tetragonal transition temperature (T_M) of those materials which are expected to exhibit tetragonal transition. These are calculated based on ΔE using the conversion factor $1 \text{ meV} = 11.6 \text{ K}$. As discussed above, these T_M values are not to be considered as the absolute values of the transition temperature. These values are listed here to only give a trend of the relative transition temperatures for different materials as has been done in the literature earlier.^{20,30} Out of the four ferromagnetic materials (magnetic aspect of the materials is discussed in detail in the next subsection) showing the possibility of a tetragonal transition, we find that Ni_2MnGa has the lowest T_M value; on the other hand, Co_2MoGa is expected to have the highest transition temperature. The optimized c/a values for all the four materials are given in Table 1. Co_2MoGa is found to have the highest value of about 1.4. Furthermore, volume conservation between the cubic and the tetragonal phases (Table 1) as well as an energetically lower tetragonal phase (Figure 5) which are observed here are generally indicative of the martensite transition. Therefore, from the present study, among the materials studied here, two Ni-based and two Co-based FHAs are likely to exhibit MSMA property.

Table 1. Martensite transition temperature of the four ferromagnetic materials^a

Material	$(c/a)_{eq}$	ΔE (meV/atom)	T_M (K)	$ \Delta V /V$ (%)
Ni ₂ MnGa	1.22	6.05	70.18	0.30
	1.22 ^b , 1.22 ^c	6.18 ^b	70.51 ^b , 210 ^d	
Ni ₂ MoGa	1.27	11.08	128.58	0.36
Co ₂ MoGa	1.37	19.58	227.13	1.96
Co ₂ NbSn	1.11	10.63	123.33	0.08
			233 ^e	

^aComparison with the experimental or theoretical data, wherever results are available

^bRef.19 ^cRef.33 ^dRef.5 ^eRef.34

Out of which one Ni and one Co-based alloys are well-known MSMA materials, namely Ni₂MnGa and Co₂NbSn. On the other hand, Co₂MoGa and Ni₂MoGa are two new materials which are also likely to exhibit martensite transition.

B. Magnetic Properties

Table 2. Magnetic properties of austenite phase of Co-based materials; Z_t is the total number of valence electrons^a

Material	μ_t	Z_t-24	μ_A	μ_B	μ_C	T_C (K)	P(%)
Co ₂ ScGa	0.00	0	0.00	0.00	0.00	-	-
	0.25 ^b						
Co ₂ TiGa	1.00	1	0.62	-0.14	-0.01	161	97
	0.75±0.03 ^c , 0.82 ^d		0.40 ^b , 0.40±0.1 ^c				
Co ₂ VGa	2.00	2	0.95	0.18	-0.01	356	100
	1.92 ^e , 2.00 ^f		0.91 ^f				
Co ₂ CrGa	3.03	3	0.77	1.59	-0.05	418	92
	3.011 ^g , 3.01 ^g		0.90 ^g				
Co ₂ MnGa	4.10	4	0.77	2.73	-0.07	586	68
	4.04 ^h						
Co ₂ YGa	0.00	0	0.00	0.00	0.00	-	-
Co ₂ ZrGa	1.00	1	0.61	-0.11	-0.01	166	94
Co ₂ NbGa	2.00	2	1.04	-0.01	0.00	397	100
	1.39 ⁱ , 2.00 ^j						
Co ₂ MoGa	2.93	3	1.22	0.51	-0.01	180	86
Co ₂ TcGa	3.95	4	1.37	1.26	-0.04	711	71
Co ₂ ScSn	1.05	1	0.67	-0.14	-0.02	207	80
Co ₂ TiSn	2.00	2	1.07	-0.06	0.00	409	100
	1.96 ^e						
Co ₂ VSn	3.00	3	1.08	0.89	-0.02	291	100
	1.21 ^e , 1.80 ^f						
Co ₂ MnSn	5.03	5	0.98	3.23	-0.06	897	76
	5.02 ^f		0.885 ^f				
Co ₂ YSn	1.05	1	0.67	-0.10	-0.02	162	79
Co ₂ ZrSn	2.00	2	1.10	-0.09	0.01	449	100
	1.46 ^e						
Co ₂ NbSn	1.98	3	0.97	0.07	0.01	37	-66
	0.69 ^e						

^aComparison with experiments or previous calculations, wherever data are available

^bRef.35; ^cRef.36; ^dRef.37; ^eRef.38; ^fRef.39; ^gRef.40 ^hRef.41 ⁱRef.42 ^jRef.43

Total and Partial Magnetic Moments - After analysing in detail the electronic stability of the austenite phase as well as the relative energetics of the martensite phase of the materials, we now discuss in detail the magnetic

properties of the cubic phase of the Ni and Co-based materials, only which are ferromagnetic in nature. The materials which are electronically unstable are not discussed further as well. As observed earlier¹⁹ for Ni₂CrGa, it is seen that Ni₂CrSn too is expected to show *intra-sublattice* anti-ferromagnetism; though in both cases, partial moment on Cr atom is seen to be significant. Further, a first-principles calculation by Sasioglu et al on a series of materials, like Pd₂MnZ, Cu₂MnZ, show that the magnetic moment is mainly confined on the Mn sublattice for these alloys which contain Mn as the *B* atom, and a very small moment is induced on the Pd or Cu atom.¹² Similarly, in the Ni-based materials studied here, the magnetism in this class of materials is expected to arise primarily due to the *B* element. This is because, by itself, Ni carries a very small magnetic moment and, Ga as well as Sn are having almost zero moment. Often the moment of the *A* atom is seen to be strongly influenced by the *B* atom as is observed in the literature^{12,47} as well as for the Ni-based alloys studied here, except the *B* = Mn materials, namely, Ni₂MnGa and Ni₂MnSn. Ni₂VSn, which has a very flat minimum in the ΔE versus c/a curve, has a very small moment as well. We find that, out of all the Ni-based materials, only two Ni₂*BC* alloys, namely, Ni₂MnGa and Ni₂MnSn exhibit the FM nature and they have very similar total moments. While the total moment is 4.10 μ_B in the former, it is 4.09 μ_B in the latter. Each of Ga and Sn has negligible moments in both cases. As for Ni atom, the moment on this atom is larger in the former alloy (0.36) compared to the latter material (0.24). Further, it is noted that Mn atom has a much larger moment in case of Ni₂MnSn (3.64) compared to the case of Ni₂MnGa (3.41). Though the common *B* atom has a difference of moment of 0.23 μ_B , due to the reasonably lower moment of the Ni atom in case of Ni₂MnSn, the total moments of these two materials are found to be very close to each other.^{45,46} These findings can be supported by the observed larger lattice parameter of Ni₂MnSn compared to that of Ni₂MnGa. Due to the larger lattice parameter in the former, the delocalization of the *3d* electrons of Mn atom is expected to decrease, leading to a larger and more atomic-like partial moment on the same. The larger lattice constant in Ni₂MnSn leads to the decrease in the overlap between the Mn and Ni atoms, as is evident from the relative DOS too, as discussed later. This may be the likely reason as to why the moment of the Ni atom decreases in case of Ni₂MnSn in comparison to Ni₂MnGa, as discussed in the literature.⁴⁶

Table 2 gives the total and partial moments for the electronically stable Co-based materials. The values available from the literature are also listed in the table for a few materials, wherever available and we note that the matching is very good with the existing calculated data. With the experimental results the matching is reasonably good. It is seen that each of Ga and Sn has negligible moments in all cases. We observe that, as opposed to the materials with *A* = Ni atom, those with *A* = Co atom have significant contribution from the *A* atom to the total moment. However, when the *B* atom is non-magnetic, in a few cases, the moment on the Co atom is zero or much less compared to its bulk moment. As the moment on the *B* atom increases, the moment of the Co atom gets larger but always largely underestimated compared to the value of its bulk moment (about 1.7 μ_B). This is expected due to the delocalized-like common d-band between the *A* and *B* atoms.¹⁰ For period IV, when *B* = Cr and Mn, there is a slight decrease in the partial moment of the Co atom, but not in the total moment value of the respective systems. For all the Co-based alloys, the moments are very close to an integer value and this is generally the signature of a half-metallic material. Further, from Table 2, we note that these FHAs follow the Slater-Pauling rule as is seen earlier in case of many Co-based FHAs.^{43,44} As a consequence of this rule, we get an almost linear variation of the magnetic moment with the atomic number of *B* elements for all the Co-based materials. It is seen that there is a deviation from the Slater-Pauling rule only for Co₂NbSn which has been observed and explained in the literature.⁴³ Due to the electronic structure, all the Co-based compounds are seen to exhibit (Table 2) a high spin polarization at the Fermi level (E_F) in comparison to the Ni-based compounds. From our calculations, Ni₂MnGa and Ni₂MnSn have spin-polarizations ~ 28 and $\sim 21\%$, respectively.

Heisenberg Exchange Coupling Parameters - To gain insight into the magnetic interactions in detail we calculate and present the results of our calculation of the Heisenberg exchange coupling parameters, J_{ij} , (*i* and *j* being pairs (*A*, *A*) and (*A*, *B*)) for the alloys which are likely to exhibit tetragonal distortion and consequently martensite transition. We also show the same parameters for some other related alloys for the purpose of comparison. Most of the materials chosen for presentation have relatively large moment on the *B* atom so that the (*A*, *B*) exchange interactions are always significant. In the left panels of Figures 6, 7 and 8, the J_{ij} parameters for different compounds are plotted. The right panels give the interaction parameters, J_{ij}^{bare} , which are J_{ij} parameters, divided by the product of the moments of the *i* and *j* atoms.

Figure 6 gives these parameters for Ni₂MnGa and Ni₂MnSn which exhibit the effect of the change of the *C* atom, and consequently the lattice parameter. Figure 7 contains the values for Co₂MnGa and Co₂MoGa to understand what is the role of the *B* = Mn over the Mo atom. Similarly, we plot the exchange parameters for alloys Co₂MnSn and Co₂NbSn in Figure 8. The results match well with the literature wherever the data are available.^{45,47} It is seen that there is a RKKY¹¹ type of interaction for the (*A*, *A*) and (*B*, *B*) pairs.^{10,12} The oscillatory behavior of the J_{ij} parameters as a function of distance between the atoms *i* and *j* (normalized with respect to the lattice constant), is a well-known signature of the same. Further, it is seen that between the *A* and the *B* atoms there is a signature of a significant direct interaction whenever *B* has a strong moment. From Figure 6, we observe that the direct interaction

between Ni-*B* atom is stronger in case of Ni₂MnGa compared to the case of Ni₂MnSn. This is due to the increased lattice constant and hence weak coupling in case of the latter. It is also found that the direct interaction is somewhat stronger than the RKKY interaction in case of both the materials, though it is quite clear that, as expected and observed in the literature^{10,12}, both these types of magnetic interactions are important in these materials.

The magnetic interactions in the Co-based materials shown here exhibit a somewhat similar trend. It is found that for the materials favoring tetragonal transition, Co₂MoGa (Figure 7) and Co₂NbSn (Figure 8), the direct *A-B* magnetic interaction is small and to some extent comparable to the indirect RKKY-type interaction between *A* atoms. In the former material, as is evident from Table 2, the moment on Mo atom is somewhat larger compared to that on the Nb atom in case of the latter material. Consequently, the strength of the direct interaction in the former alloy, between *B* atom (Mo) and *A* atom (Co) is found to be slightly more. From Figures 7 and 8, we observe that for the materials Co₂MnGa and Co₂MnSn, having high magnetic moments (4.10 and 5.03 μ_B , respectively), which are of the order of the moments possessed by the two Ni-based materials discussed above, the direct *A-B* interaction is much stronger compared to the RKKY-type indirect interactions (*A-A* or *B-B*). A decrease of partial moment of the Mn atom is observed in case of Co₂MnGa over Ni₂MnGa (2.73 in Co₂MnGa versus 3.41 μ_B in Ni₂MnGa). But due to larger moment on the *A* = Co over Ni atom, the direct interaction strength between Mn and the respective *A* atoms, is much larger in the former material, as seen from top left panels of Figures 6 and 7. Hence, the delocalized common 3*d* band between Mn and Co atom in case of Co₂MnGa is expected to be more effective compared to the case of Ni₂MnGa. We observe from Figures 6,7 and 8 that, relatively, the RKKY-type indirect interactions are slightly stronger for the *C* = Sn over Ga atom. It is to be noted here that Sn atom has one valence electron more than Ga.

It is known that the magnetic interactions in the Heusler alloy materials having a large moment on *B* atom, comprise of a large contribution from the *A-B* direct interaction. At the same time, contribution of the the *A-A* and *B-B* indirect RKKY type of interaction is important as well. The materials, which have high moment on the *B* atom, typically exhibit a large *A-B* direct interaction when compared to the strength of RKKY-type interaction. However, when the J_{ij}^{bare} parameters are analyzed, for the majority of the materials, it is seen that, both the direct *A-B* interaction and RKKY-type interaction between *i* and *j* (*i* and *j* being *A* and *B*) atoms, are somewhat similar in strength. This observation reiterates the fact that the magnetic exchange interactions are not only the function of *i-j* distances (as is evident from Figures 6 to 8), but also of the individual magnetic moments of the *i* and *j* atoms which becomes clear when we present the J_{ij}^{bare} plots.

Based on the J_{ij} parameters of the six materials discussed above, the Curie temperatures of the materials within a mean-field approximation²⁷ have been calculated to probe further into the possible MSMA property. For Ni₂MnGa and Ni₂MnSn, the Curie Temperature (T_C) values are 410 and 365 K, respectively. These values as well as the J_{ij} parameters match quite well with both experimental and calculated values reported in the literature.^{45,47} We note that the experimental values are generally underestimated compared to the theoretical values. This is because of the mean-field-approximation. For some of the Co-based materials T_C values are presented in Table 2. We observe that the calculated values match very well with the previously reported data, wherever these results are available. It is interesting to note that due to the small values of J_{ij} for Co₂NbSn the value of the Curie temperature for this material is very low and this is consistent with the experimentally observed room-temperature paramagnetism in this material. Similarly, due to weak RKKY-type interaction of pair (*A*, *A*) with a somewhat comparable *A-B* direct interaction, the T_C value for another Co-based material, which has been predicted from our present work, namely, Co₂MoGa, is expected to be below room temperature as well.

C. Bulk Mechanical Properties

Table 3. Bulk mechanical properties of austenite phase of Ni-based materials^a

Material	C ₁₁ (GPa)	C ₁₂ (GPa)	C ₄₄ (GPa)	C'(GPa)	B(GPa)	G _V (GPa)	G _R (GPa)	G _V /B
Ni ₂ VGa	193.20	183.32	109.36	4.94	186.62	67.59	11.56	0.36
Ni ₂ MnGa	165.41	159.45	113.67	2.98	161.44	69.39	7.16	0.43
	152.0 ^b	143 ^b	103 ^b	4.5 ^b	146 ^b	63.6 ^b		
Ni ₂ MoGa	197.36	206.36	103.40	-4.5	203.36	60.24	-12.04	0.30
Ni ₂ MnSn	161.02	137.46	92.56	11.78	145.31	60.25	24.73	0.41
	158.1 ^c	128.5 ^c	81.3 ^c , 87 ^d	14.8 ^c , 8 ^d	138.4 ^c , 140 ^d			

^aComparison with experiments or previous calculations, wherever data are available

^bRef.48 ^cRef.49 ^dRef.46

After presenting the results of magnetic properties of the austenite phase of the materials, now, we discuss about the

Table 4. Bulk mechanical properties of austenite phase of Co-based materials^a

Material	C ₁₁ (GPa)	C ₁₂ (GPa)	C ₄₄ (GPa)	C'(GPa)	B(GPa)	G _V (GPa)	G _R (GPa)	G _V /B
Co ₂ VGa	266.52	162.12	126.83	52.20	196.92 198 ^b	96.98	80.68	0.49
Co ₂ CrGa	233.02	182.82	136.77	25.1	199.56	92.10	49.20	0.46
Co ₂ MnGa	254.87	165.27	142.69	44.80	195.14 199 ^c	103.53	76.14	0.53
Co ₂ MoGa	180.92	163.60	114.10	8.66	169.38	71.92	19.44	0.42
Co ₂ TcGa	249.54	186.10	123.87	31.72	207.25	87.01	57.29	0.42
Co ₂ MnSn	234.63	136.75	119.05	48.94	169.38	91.01	75.68	0.54
Co ₂ NbSn	164.95	184.99	80.80	-10.02	178.31	44.47	-30.77	0.25

^a Comparison with experiments or previous calculations, wherever data are available

^bRef.50 ^cRef.46

bulk mechanical properties of the same phase since from technological application point of view, these properties are important. For demonstrating the differences, we concentrate on eight typical FM materials and present the detailed results of the same. Three of these FM materials are likely to undergo a tetragonal distortion at low temperature and these materials are Ni₂MnGa, Co₂MoGa, Co₂NbSn. The other group of alloys consists of materials having a cubic ground state. Among these alloys, the following compounds have been considered - Co₂VGa, Co₂CrGa, Co₂MnGa, Co₂MnSn and Ni₂MnSn, which are expected to have a cubic symmetry at the lowest temperature. Tables 3 and 4 contain the bulk mechanical properties of these above-mentioned Ni and Co-based alloys, respectively. Values of few other materials are also listed in Tables 3 and 4, for comparison. It is observed that the overall agreement with the values from the literature is reasonably good.

There are three independent elastic constants for a cubic structure. These are C₁₁, C₁₂ and C₄₄. These three elastic constants can be found by calculating energies for three different types of strain on the unit cell of the system under equilibrium. From these three linearly independent energy versus strain data, we can find out C₁₁, C₁₂ and C₄₄. The applied strains have the form as ($\delta, \delta, \delta, 0, 0, 0$), ($0, 0, 0, \delta, \delta, \delta$) and ($\delta, \delta, (1+\delta)^{-2}-1, 0, 0, 0$). δ has been taken in the range of -0.02 to +0.02 in steps of 0.005. To start with, we calculate the equilibrium lattice parameter (a_0) as well as equilibrium volume (V_0), and the corresponding energy is considered as the equilibrium energy (E_0). Then strain is applied to the system. Under this strained condition, the energy (E) is calculated and subsequent to that, the elastic constants are obtained from our calculations as discussed below. The energies $\frac{E-E_0}{V_0}$ are plotted as a function of applied strain and fitted with a fourth order polynomial. The second order coefficient of the fit gives the elastic constants. The mechanical stability criteria for the cubic crystal are as follows: C₁₁ > 0, C₄₄ > 0, C₁₁-C₁₂ > 0 and C₁₁+2C₁₂ > 0. From the tables containing elastic constants we can see that first, second and fourth conditions are satisfied for all the materials listed here, but the third condition is not satisfied by some of the materials.

Tetragonal shear constant (C') - This is defined as $0.5 \times (C_{11} - C_{12})$. A value of C' which is close to zero or negative indicates that the material is mechanically unstable and prone to tetragonal distortion. It is clear from Table 3, that for Ni₂MnGa, as expected, the tetragonal shear constant is quite close to zero. For Ni₂MoGa the value of C' is found to be negative, which indicates that it has a mechanically unstable cubic austenite phase, which corroborates the result presented in Figure 5. It is interesting to note that Ni₂VGa has a value of C' close to that of Ni₂MnGa. From Figure 5, we observe that it has a flat region near $c/a = 1$, in the energy versus c/a curve. Hence, in this case the ground state symmetry can not be properly ascertained as is evident from our results. It is important to mention here that the stoichiometric Ni₂MnSn is a material which is not known to undergo martensite transition and we find that the tetragonal shear constant has a slightly larger positive value of about 12 compared to Ni₂MnGa.

From Table 4, it is observed that two Co-based materials show a negative or close to zero value for C'. Out of these, Co₂NbSn is known to exhibit non-cubic distortion.²⁹ Among the materials, namely, Co₂MoGa, Co₂VGa, Co₂CrGa, Co₂CrGa, Co₂MnSn, Co₂TcGa, except the first alloy all others have a large positive value for the C' constant. It is also observed from Figure 5 that, for Co₂MoGa, there is a clear indication of the tetragonal phase being the lowest energy state. This is not the case for the other materials. So the combined study of energetics and bulk mechanical properties of all the materials⁵¹ indicates that the only two Co₂BC materials which are likely to undergo tetragonal transition and to exhibit SMA property are Co₂NbSn and Co₂MoGa.

Inherent Crystalline Brittleness (ICB) - The calculated values of bulk modulus, B, have been listed in Tables 3 and 4 for Ni and Co-based materials, respectively. The isotropic shear modulus, G, is related to the resistance of the material to the plastic deformation. In literature, it has been shown⁵² that the value of G lies in between the values of shear moduli given by formalisms of Voigt (G_V)⁵³ and Reuss (G_R)⁵⁴, which means $G = (G_V + G_R)/2$. As has been discussed for austenite phase of Ni₂MnGa in our previous work (Ref.14) the experimental G value is close to

the calculated G_V value while G_R value remains largely underestimated. This occurs due to the small positive value of C' . This particular aspect of similar FHAs, showing martensite transition, has already been discussed in detail in the literature.¹⁴ Following this observation, we consider G_V value as the value of shear modulus (G) though it is generally considered to be the higher limit of the same. Further, a simple and empirical relationship, given by Pugh⁵⁵, proposes that the plastic property of a material is related to the ratio of the shear and bulk modulus of that particular material. A high value (greater than ~ 0.57) of ratio of shear and bulk modulus, namely, G/B , is connected with the inherent crystalline brittleness of a bulk material. A value below this critical number phenomenologically signifies that the material's ICB is low. From Table 3, we find that the values for Ni-based materials are below this critical value and hence the ICB of these materials is low though the well-known FHA, Ni₂MnGa, has a somewhat higher value compared to the materials containing platinum in place of Ni.¹⁴ We note that Ni₂MoGa show a negative value of C' , as well as the lowest value of G/B among all and hence it is expected to have a low ICB. So from energetics (Figure 5) and bulk mechanical points of view, it is a promising material, though not from magnetic point of view. Table 4 lists the bulk mechanical properties for the Co-based FHAs studied here. The two materials which are likely to show a tetragonal ground state (namely, Co₂NbSn and Co₂MoGa) are expected to exhibit ICB smaller or comparable to Ni₂MnGa ($G/B = 0.25$ and 0.42 , respectively). All the rest of the Co₂BC alloys have G/B values comparable to or larger than that of Co₂NbSn.

Cauchy Pressure - We now focus on the value of Cauchy Pressure, C^p , which is defined as $C^p = C_{12} - C_{44}$. In Figure 9, we plot the available data for C^p versus G_V/B calculated in case of some of the Ni and Co-based compounds. We find that overall, there is a clear trend of inverse (linear) relationship between G_V/B and C^p . In the literature also, it is observed that, the higher the C^p , the lower the ratio G/B . Interestingly, this type of nearly-linear inverse relationship between the Cauchy pressure and the G/B ratio seems to be a rather general observation as observed in the literature for various types of materials.^{14,56}

Finally, after analyzing the bulk mechanical as well as the magnetic properties and the energetics, out of all the materials studied, only two new materials, namely, Ni₂MoGa and Co₂MoGa, emerge to be promising in terms of application as an SMA material. However, due to the absence of any magnetic moment in Ni₂MoGa, this material is not expected to be suitable as an MSMA material. A low T_C indicates an absence of ferromagnetism in Co₂MoGa at room temperature as is observed in case of Co₂NbSn.

D. Electronic Properties: Density of States

1. Analysis of Total and Atom-Projected Partial DOS

After discussing the energetics, magnetic and bulk mechanical property of the cubic austenite phase, we now analyse the electronic property in terms of the total and partial density of states of different atoms of various materials. We have carried out calculations on all the electronically stable materials⁵¹ but here we concentrate on and present the results of the austenite phases of eight typical FM materials as discussed above. These materials are Ni₂MnGa, Co₂MoGa, Co₂NbSn, which are to exhibit a tetragonal symmetry as well as Co₂VGa, Co₂CrGa, Co₂MnGa, Co₂MnSn and Ni₂MnSn, which are to possess a cubic symmetry, at the lowest possible temperature. We will discuss the total and atom-projected DOS of these systems in this section.

Total DOS:

It is seen that the valence band width for all the materials is about the same, which is roughly about 6 eV (Figures 10 to 13). The two-peak structure in the DOS for both Ni and C atoms indicating about substantial hybridization among these atoms is evident from Figure 10. A two-peak structure is observed at the Fermi level, this indicates a strong hybridization between the Ga and Ni atoms. This covalent interaction between the Ga 4*p* and Ni 3*d* minority electrons plays a crucial role in the stability. We note here that the overlapping and the two-peak structure of the DOS is prominent in case of A and C atoms of Co₂ZrGa, which has a highly negative formation energy (Figure 4). On the other hand, in Co₂CrGa, the two-peak structure and the overlapping of DOS for both the A and C atoms are not quite substantial and the formation energy is low as well (Figure 4).⁵¹ Further, Figure 13 depicts the DOS for B = Y and Zr. These plots indicate a lowering of binding energy in the B = Zr material compared to the B = Y case. This corroborates the trend of the formation energy values of these materials. It is to be noted that the contribution from the A atom plays a crucial role in this. Zayak et al¹³ have earlier shown that the stability of the Ni₂MnGa type Heusler alloys is closely related to the minority DOS at the Fermi level as has been argued in other cases as well.⁵⁷

There is a large exchange splitting observed for systems which have Mn as the B atom. From Figures 10 to 12, we observe that for A₂BC systems (A = Ni, Co; B = Mn; C = Ga; Sn), the occupied DOS of the B atom is dominated by the majority spin whereas the unoccupied DOS is dominated by the minority spin. For Ni₂MnGa and Ni₂MnSn, the majority DOS of the Mn atom is centred around -1.2 eV and -1.5 eV, whereas the minority DOS of the same atom is centred around 1.5 eV and 1.3 eV for the respective systems. For Co₂MnGa and Co₂MnSn, the position

of the occupied majority spin DOS for Mn atom is at about -0.7 eV and -1.1 eV, respectively, while the position of the unoccupied minority DOS peak is at about 1.8 eV and 1.6 eV. For Co_2CrGa also, we observe a large separation between the occupied majority DOS peak (at about -0.1 eV) of Cr atom and unoccupied minority DOS peak (at about 1.7 eV). Next, we analyze the partial DOS of few of the important A , B atoms, to understand the nature of DOS close to the Fermi level.

Partial DOS :

Ni Atom - The DOS in case of the two Ni-based alloys are similar (Figure 10). However, since Sn atom contains one extra valence electron compared to the Ga atom in the C position, the peak positions of the total DOS of the Mn atom are shifted towards lower energy in case of the materials with $C = \text{Sn}$. At this point, it is worth-mentioning that it has already been discussed in the literature that a rigid band model is a suitable model to understand the trends when the C atom is changed.⁴⁶ We further observe that a similar situation is seen to arise when the A atom is changed from Ni to Co, which is discussed below.

Co Atom - Co has one valence electron less than Ni. Hence, a larger contribution of Co-derived levels compared to Ni-derived levels in the unoccupied part of the respective DOS is expected. Figures 11 to 13 depict this. When DOS of Ni_2MnCa is compared with $\text{Co}_2\text{Mn}C$, it is clearly evident (Figures 10, 11 and 12). Among the materials with $C = \text{Ga}$ and $A = \text{Co}$, only Co_2MoGa is a material which is likely to show a martensite transition (Figure 5). It is seen that it has the first unoccupied DOS peak very close to the E_F (Figure 11). Among the materials with $C = \text{Sn}$ and $A = \text{Co}$, only Co_2NbSn is known to be prone to distortion²⁹ and it has an unoccupied DOS peak close to E_F as well. When we analyze the DOS of Co_2MnGa (Figure 11) and Co_2MnSn (Figure 12), which do not show the tendency of a tetragonal distortion as well as are known to possess high spin polarization at the Fermi level, we observe that the first unoccupied DOS is further away from E_F compared to the materials which are prone to tetragonal distortion, namely Co_2MoGa (Figure 11) and Co_2NbSn (Figure 12).

Mn Atom - There are four out of eight materials which contain Mn atom in the B position. When we compare the total DOS of the Mn atom at the B position, in all the four materials considered here, it is clearly seen that majority of the DOS of the down spin occupies the unoccupied region above the Fermi level, while the up spin electrons primarily have negative binding energies. As opposed to the down spin DOS, which has one major peak in all the four cases, the up spin electrons typically occupy two energy ranges, one around 1 and one around 3 eV below E_F . Due to one extra electron in Sn atom compared to the Ga atom in the C position, the peak positions of the total DOS of the Mn atom are shifted towards lower energy in case of the materials with $C = \text{Sn}$. To elaborate, first we compare the DOS of the up spin of Mn in the four alloys Ni_2MnGa , Ni_2MnSn , Co_2MnGa and Co_2MnSn in the cubic phase. While DOS of Mn atom in the unoccupied part peaks at about 1.5 eV in case of $C = \text{Ga}$, it peaks around 1.2 eV when $C = \text{Sn}$. The corresponding peak positions for Co_2MnGa and Co_2MnSn are at about 1.8 and 1.6 eV, respectively. In case of the up spin DOS, there are two ranges of predominant DOS in all the four materials. For the first such range, which is closer to the Fermi energy, the peak positions are at about -1.3, -1.5, -0.7 and -1.1 for Ni_2MnGa , Ni_2MnSn , Co_2MnGa and Co_2MnSn , respectively. For the range which is at a much higher binding energy, the peak positions are at about -3.2, -3.2, -2.5 (also one slightly weaker one at -2.8) and -2.5 (also one slightly weaker one at -2.8) eV for Ni_2MnGa , Ni_2MnSn , Co_2MnGa and Co_2MnSn , respectively. It is to be noted that the peaks of the DOS are not sharp but broad ones, with shoulders on either or one of the sides.

2. Electronic Stability of the Tetragonal phase from DOS

After discussing the electronic property of the cubic austenite phase, we now analyse the electronic property in terms of the density of states of different materials as a function of c/a . We concentrate on the eight typical FM materials as discussed above. A tetragonal distortion has been imposed on all these eight materials. To highlight the difference between the two symmetries, we will concentrate on the detailed results of cases with $c/a = 1, 1.05$ and 1.10 . The aim is to understand the electronic stability or instability of the tetragonal phase of these compounds from the DOS results.

Ni_2MnGa versus Ni_2MnSn :

Figure 14 contains the density of states of the cubic and tetragonal phases, with c/a varying from 1 to 1.10 in steps of 0.05 for materials Ni_2MnGa and Ni_2MnSn . First we will analyse Figure 14 for the cubic phase. We observe that there is a peak at around -0.2 eV for Ni_2MnGa and at around -0.5 eV for Ni_2MnSn , respectively. As has been established in the literature, this peak, which is close to the E_F , has negative binding energy. This peak is derived from the electrons of the Ni atoms with down spin having e_g symmetry and is known to play a crucial role in the stabilization of the tetragonal phase in case on Ni_2MnGa .⁴⁶ The density of states of the down spin electrons with t_{2g} symmetry of these A atoms corresponds to the peaks with reasonably higher binding energy. This is the case for both the materials. On the other hand, detailed investigation suggests that the B atom = Mn has negligible contribution near the Fermi level; both for the up and for the down spin. The up spin electrons of A atom also do not significantly

contribute to the DOS at around -0.2 and -0.5 eV for Ni₂MnGa and Ni₂MnSn, respectively.

As c/a increases in case of these materials, there are some systematic changes in the density of states, clearly visible from the lower panels of the Figures 14 to 17. For Ni₂MnGa, it is seen that the peak near the Fermi level, at about -0.2 eV, derived from the down spin DOS, has been split into two peaks. This has been observed and argued about in detail in the literature.^{46,58,59} As a result of tetragonal distortion, the degeneracy of the sub-bands near the Fermi level is lifted. As a consequence, a redistribution of the density of states of the 3*d* electrons and in turn a reduction of free energy occurs. This is the so-called band Jahn-Teller effect which is known to result in the lowering of energy under tetragonal distortion in many FHAs including Ni₂MnGa.^{46,58} For Ni₂MnSn as well, it is seen that the most prominent change being the splitting of the peak at about -0.5 eV⁴⁶ upon the tetragonal distortion as seen from Figure 14. However, it is well-known that stoichiometric Ni₂MnSn is not expected to have tetragonal ground state. It has been argued in the literature that the band Jahn-Teller effect is sensitive to the DOS at the E_F in the cubic phase. The closeness of the degenerate peak for Ni₂MnGa (at about -0.2 eV with respect to E_F) over Ni₂MnSn (at about -0.5 eV below E_F) is an indication of the possibility of tetragonal distortion in the former.^{46,58} We find that the density of states at E_F in case of cubic phase of Ni₂MnGa is relatively more in comparison to Ni₂MnSn, which is evident from the relative position of the e_g peak near the Fermi level in the two materials (Figure 14).

Co₂MoGa versus Co₂MnGa :

Figure 15 gives the plot of DOS with different c/a values. We note that in the literature the stability of the martensite phase for a Co-based system (Co₂NiGa) has been explained to be due to the lowering of energy of the system under the tetragonal deformation compared to the cubic structure.⁶⁰ In case of Co₂MoGa there is a large peak in the minority DOS just above the Fermi level (at about +0.3 eV with respect to E_F). Detailed analysis shows that this peak at the minority DOS has contributions from all three atoms i.e. (Co, Mo, Ga), but the major contribution comes from the e_g levels of 3*d* electrons of Co. We find that these Co e_g levels have a major role in the stabilization of the tetragonal phase, similar to the Ni e_g levels in case of Ni₂MnGa. Hence, in case of Co₂MoGa also, band Jahn-Teller distortion plays a significant role. The down spin DOS close to the Fermi level is high, which leads to the instability of the cubic phase of this material unlike Co₂MnGa. In case of the latter material, the minority DOS almost vanishes at E_F . Further, here, the e_g levels of Co atom are located farther away from the Fermi level (at about +1.0 eV with respect to E_F). For both the materials *B* atom does not contribute to the minority DOS at the Fermi level. However, primarily the *B* atom only contributes significantly to the large DOS of the up spin electrons at the Fermi level for Co₂MoGa. The peak positions of the DOS in the unoccupied part of the energy for Co₂MoGa and Co₂MnGa are different due to the hybridization of Co atom with the Mo and Mn atoms, respectively. This led to the difference in the electronic characters of these two materials.

Co₂NbSn versus Co₂MnSn :

Figure 16 gives the plot of DOS with different c/a values. As in case of Ni₂MnGa, for Co₂NbSn also we can find same type of evolution of density of states as a function of c/a and Co 3*d* e_g states play the key role in the tetragonal transition. In austenite phase of Co₂NbSn the Co 3*d* e_g peak is at just above Fermi level (at about +0.05 eV). Under tetragonal distortion this peak is split into two: one part being above the Fermi level and another one being below the Fermi level. This splitting lowers the energy of the system and the tetragonal phase tends to be the ground state structure compared to the cubic structure. In the literature²⁹, it has been observed that at the Fermi energy, the contribution to DOS mainly comes from the 3*d* bands of Co and Nb. We observe from Figure 12 that Sn atoms also contribute. In the cubic phase Co atom has a single large peak just above the E_F . But under tetragonal distortion, this single peak is split into two and the energy of the tetragonal phase is lower compared to the cubic phase. It has been observed²⁹ that the band Jahn-Teller distortion is the cause of the structural transition. As seen from Figures 12 and 16, for Co₂MnSn, the peak due to Co 3*d* e_g levels is located at a higher energy (at about +0.8 eV) compared to Co₂NbSn. After the application of the tetragonal distortion this single peak is split into two (Figure 16). But in this case after splitting both the peaks lie above E_F which does not yield to lowering of energy.

Co₂CrGa versus Co₂VGa :

From Figure 17, it is observed that the single peak of the Co 3*d* e_g above E_F is split for Co₂VGa. However, after splitting both the peaks lie above E_F . So there is no lowering of energy of the system possible under tetragonal deformation. For Co₂CrGa, the Co 3*d* e_g single peak of cubic phase is located at an even higher (positive) energy with respect to the Fermi level. In this case also lowering of energy under tetragonal deformation is not possible, which is consistent with the results presented in Figure 5.

Finally, we find that in all the materials, as a result of tetragonal distortion, the degeneracy is lifted for the 3*d* sub-bands in the minority spin channel of *A* atoms, present closest to the Fermi level. Subsequently, as a result of this band Jahn-Teller effect, a redistribution of the density of states of these 3*d* electrons occurs. In all the materials, which favor a tetragonal deformation, a substantial density of states very close to the Fermi level has been observed. In other words, the band Jahn-Teller effect is found to be, as expected, quite sensitive to the DOS at or close to the E_F in the cubic phase. As a result of the redistribution of the DOS, under tetragonal distortion, due to closeness of peak in DOS to the E_F , the energy gets lowered in these materials. Consequently, the possibility of martensite

transition is found to be high. Further, for these materials, a negative or very close to zero value of tetragonal shear constant, C' , has also been observed, as is expected from the literature. For all the other materials, under tetragonal distortion, the splitting of the $3d$ minority spin levels is observed as well but the peak is away from the E_F resulting in a reduced density of states at E_F . Therefore, the lowering of free energy is not possible, which renders the tetragonal transition unlikely. The observation regarding the cubic ground state for these materials is further corroborated by the relatively large and positive values of C' for all these materials.

IV. SUMMARY AND CONCLUSION

It has been of particular interest that out of all the Ni and Co-based full-Heusler alloys studied so far in the literature, only some materials undergo the martensite transition and these generally show the technologically important magnetic shape memory alloy property. These full Heusler alloys in general are found to be metallic in nature. On the other hand, it has been observed that there is another group of FHAs which are half-metallic-like in nature, with a much reduced density of states at the Fermi level in case of one of the spin channels and these materials generally do not exhibit MSMA property. It has been observed earlier that while most of the Ni-based FHAs show MSMA property, many of the Co-based FHAs exhibit large spin-polarization at the Fermi level.

Therefore, in this paper, using first-principles calculations based on density functional theory, we study in detail the bulk mechanical, magnetic and electronic properties of a series of Ni and Co-based full Heusler alloys, namely, Ni_2BC and Co_2BC ($B = Sc, Ti, V, Cr$ and Mn as well as Y, Zr, Nb, Mo and Tc ; $C = Ga$ and Sn). After establishing the electronic stability from the formation energy and subsequent full geometry optimization, we carry out the calculation of different properties to probe and understand, the similarities and differences in the properties of these materials. We analyze the data in detail to see if among these materials there is any FHA which has a tendency to undergo a tetragonal transition and at the same time possesses a high spin polarization at the Fermi level.

Out of all the electronically stable compounds of the total forty Ni and Co-based materials, most of the Ni-based materials are expected to show a non-magnetic ground state. On the other hand, Ni_2MnGa and Ni_2MnSn as well as all the Co-based materials are ferromagnetic in nature. Further, from the Heisenberg exchange interaction parameters, it is seen that the materials exhibit similar nature in terms of the relative contributions of the direct and RKKY-type nature of the magnetic interactions. The trend of the calculated values of Curie temperature for various materials, obtained from the J_{ij} parameters, matches reasonably well with the literature wherever data are available. From the point of view of bulk mechanical properties, the values of tetragonal shear constant show consistent trend: high positive for materials not prone to tetragonal transition and low or negative for others. A general trend of nearly-linear inverse relationship between the Cauchy pressure and the G/B ratio is predicted for both the Ni and Co-based materials.

It is observed that the Ni-based materials are typically metallic in nature. However, all the Co-based alloys exhibit a significant spin polarization at the Fermi level. Most of the Ni-based materials have a $3d$ band of the minority spin of the A atoms close to and below the E_F . On the other hand, the peak position of the same band is above the E_F for the Co-based materials. We observe that, in both the cases of Ni and Co-based materials, these $3d$ levels play an important role in deciding the ground state. Further, the replacements of the A, B, C sites of the A_2BC materials by different atoms, indicate that in general a rigid band model explains the differences in the electronic structure of both the Ni and Co-based materials to a large extent. This model along with the hybridization between atoms, further supports the results of partial and total moments of these systems. The relation between the closeness of the peak corresponding to the e_g levels of the $3d$ down spin electrons of the A atom to the E_F and the tendency of lowering of energy upon tetragonal distortion is consistent across all the Ni and Co-based materials.

Finally, from our study on the two categories of materials, it is clear that out of all the materials which we study here, only four FHAs show a tendency of undergoing martensite transition. Out of these four materials, which have a conventional Heusler alloy structure and exhibit a clear possibility of finding a tetragonal phase as their ground state, three of them, namely, Ni_2MnGa , Ni_2MoGa and Co_2NbSn have a metallic nature as is observed in case of majority of the MSMA material; on the other hand, from our calculations, Co_2MoGa is expected to emerge as a *shape memory alloy with high spin polarization at the Fermi level*. This interesting finding awaits a suitable experimental validation.

V. ACKNOWLEDGMENTS

Authors thank P. D. Gupta, P. A. Naik and G. S. Lodha for facilities and encouragement throughout the work. The scientific computing group, computer centre of RRCAT, Indore and P. Thander are thanked for help in installing and support in running the codes. S. R. Barman, A. Arya, S. B. Roy and C. Kamal are thanked for discussion.

TR thanks HBNI, RRCAT for financial support.

-
- ¹ P. J. Webster, K. R. A. Ziebeck, S. L. Town, M. S. Peak, *Phil. Mag. B*, **49**, 295 (1984).
- ² K. Ullakko, J. K. Huang, C. Kantner, R. C. O’Handley, and V. V. Kokorin, *Appl. Phys. Lett.* **69**, 1966 (1996).
- ³ S. J. Murray, M. Marioni, S. M. Allen, R. C. O’Handley, T. A. Lograsso, *Appl. Phys. Lett.* **77**, 886 (2000).
- ⁴ A. Sozinov, A. A. Likhachev, N. Lanska, and K. Ullakko, *Appl. Phys. Lett.* **80**, 1746 (2002); A. Sozinov, N. Lanska, A. Soroka, and W. Zou, *Appl. Phys. Lett.* **102**, 021902 (2013).
- ⁵ C. Biswas, R. Rawat, S. R. Barman, *Appl. Phys. Lett.*, **86**, 202508 (2005).
- ⁶ F. X. Hu, B. Shen, J. Sun, *Appl. Phys. Lett.*, **76**, 3460 (2000); F. X. Hu, J. Sun, G. Wu, B. Shen, *J. Appl. Phys.*, **90**, 5216 (2001).
- ⁷ S. Amari, R. Mebsout, S. Mecabih, B. Abbar, B. Bouhafs, *Intermetallics*, **44**, 26 (2014); Y. Wu, B. Wu, Z. Wei, Z. Zhou, C. Zhao, Y. Xiong, S. Tou, S. Yang, B. Zhou, Y. Shao, *Intermetallics*, **53**, 26 (2014); B. Kong, X. R. Chen, J. X. Yu, C. L. Cai, *J. Alloys and Comp.*, **509**, 2611 (2011); V. Kanchana, G. Vaitheeswaran, Y. Ma, Y. Xie, A. Svane, O. Eriksson, *Phys. Rev. B*, **80**, 125108 (2009); L. Banisla, A. I. Mallick, M. M. Raja, A. K. Nigam, B. S. D. C. S. Varaprasad, Y. K. Takahashi, A. Alam, K. G. Suresh, K. Hono, *Phys. Rev. B*, **91**, 104408 (2015).
- ⁸ R. A. de Groot, F. M. Mueller, P. G. van Engen, K. H. J. Buschow, *Phys. Rev. Lett.*, **50**, 2024 (1983).
- ⁹ W. E. Pickett, J. S. Moodera, *Physics Today*, **54**, 39 (2001).
- ¹⁰ J. Kübler, A. R. Williams, C. B. Sommers, *Phys. Rev. B*, **28**, 1745 (1983).
- ¹¹ M. A. Ruderman and C. Kittel, *Phys. Rev.*, **96**, 99 (1954); T. Kasuya, *Prog. Theor. Phys.*, **16**, 45 (1956); K. Yosida, *Phys. Rev.*, **106**, 893 (1957).
- ¹² E. Sasioglu, L. M. Sandratskii, P. Bruno, *Phys. Rev. B*, **77**, 064417 (2008).
- ¹³ A. T. Zayak, P. Entel, K. M. Rabe, W. A. Adeagbo, M. Acet, *Phys. Rev. B*, **72**, 054113 (2005).
- ¹⁴ T. Roy, M. E. Gruner, P. Entel, A. Chakrabarti, *J. Alloy. and Comp.*, **632**, 822 (2015) and references therein.
- ¹⁵ G. D. Liu, J. L. Chen, Z. H. Liu, X. F. Dai, G. H. Wu, B. Zhang, X. X. Zhang, *Appl. Phys. Lett.*, **87**, 262504 (2005); G. D. Liu, X. F. Dai, S. Y. Yu, Z. Y. Zhu, J. L. Chen, G. H. Wu, H. Zhu, J. Q. Xiao, *Phys. Rev. B*, **74**, 054435 (2006).
- ¹⁶ S. R. Barman, S. Banik, A. K. Shukla, C. Kamal, Aparna Chakrabarti, *Euro. Phys. Lett.*, **80**, 57002 (2007); S. R. Barman, Aparna Chakrabarti, *Phys. Rev. B*, **77**, 176401 (2008); S. Singh, M. Maniraj, S. W. D’Souza and S. R. Barman, *Appl. Phys. Lett.*, **96**, 081904 (2010).
- ¹⁷ K. R. Priolkar, P. A. Bhoje, D. N. Lobo, S. W. D’Souza, S. R. Barman, A. Chakrabarti, S. Emura, *Phys. Rev. B*, **87**, 144412 (2013).
- ¹⁸ I. Galanakis, E. Sasioglu, *Appl. Phys. Lett.*, **98**, 102514 (2011).
- ¹⁹ T. Roy, A. Chakrabarti, *J. Mag. and Mag. Mater.*, **401**, 929 (2016).
- ²⁰ M. Siewert, M. E. Gruner, A. Hucht, H. C. Herper, A. Dannenberg, A. Chakrabarti, N. Singh, R. Arroyave, P. Entel, *Adv. Eng. Mat.*, **14**, 530 (2012).
- ²¹ G. Kresse, J. Furthmüller, *Phys. Rev. B*, **54**, 11169 (1996); G. Kresse, D. Joubert, *Phys. Rev. B*, **59**, 1758 (1999); VASP 5.2 programme package is fully integrated in the MedeA platform (Materials Design, Inc.) with a graphical user interface enabling the computation of the properties.
- ²² P. E. Blochl, *Phys. Rev. B*, **50**, 17953 (1994).
- ²³ J. P. Perdew, K. Burke, M. Ernzerhof, *Phys. Rev. Lett.*, **77**, 3865 (1996).
- ²⁴ P. Blaha, K. Schwartz, G. K. H. Madsen, D. Kvasnicka and J. Luitz, WIEN2K, An Augmented Plane Wave plus Local Orbitals Program for Calculating Crystal Properties, (Karlheinz Schwarz, Tech. Universität, Wien, Austria), 2002, ISBN 3-9501031-1-2.
- ²⁵ A. I. Liechtenstein, M. I. Katsnelson, V. P. Antropov, V. A. Gubanov, *J. Magn. Magn. Mater.*, **67**, 65 (1987).
- ²⁶ The Munich SPR-KKR package, version 5.4, H. Ebert et al; <http://olymp.cup.uni-muenchen.de/ak/ebert/SPRKKR>.
- ²⁷ M. Meinert, J. M. Schmalhorst, G. Reiss, *J. Phys. : Cond. Matt.*, **23**, 036001 (2011); M. Meinert, J. M. Schmalhorst, G. Reiss, *J. Phys. : Cond. Matt.*, **23**, 115005 (2011) and the references therein.
- ²⁸ Michael Gillessen, "Maßgeschneidertes und Analytik-Ersatz Über die quantenchemischen Untersuchungen einiger ternärer intermetallischer Verbindungen", PhD thesis, University of Aachen, (2009).
- ²⁹ S. Fujii, S. Ishida, *J. Phys. Soc. Jpn.*, **58**, 3657 (1989).
- ³⁰ S. R. Barman, A. Chakrabarti, S. Singh, S. Banik, S. Bhardwaj, P. L. Paulose, B. A. Chalke, A. K. Panda, A. Mitra, A. M. Awasthi, *Phys. Rev. B*, **78**, 134406 (2008) and references therein.
- ³¹ M. Baral, S. Banik, A. Chakrabarti, D. M. Phase, T. Ganguli, *J. Alloys and Comp.*, **645**, 117 (2015) and references therein.
- ³² Y. Kurtulus, R. Dronskowski, G. D. Samolyuk, V. P. Antropov, *Phys. Rev. B*, **71**, 014425 (2005).
- ³³ M. B. Sahariah, S. Ghosh, C. S. Singh, S. Gowtham, R. Pandey, *J. Phys. : Cond. Matt.*, **25**, 025502 (2013).
- ³⁴ V. N. Antonov, B. N. Harmon, L. V. Bekenov, A. P. Shpak, A. N. Yaresko, *Phys. Rev. B*, **71**, 174428, (2005).
- ³⁵ A. W. Carbonari, R. N. Saxena, W. Pendl, J. Mestnik Filho, R. N. Attili, M. Olzon-Dionysio, S.D. de Souza, *J. Magn. Magn. Mater.* **163**, 313, (1996).
- ³⁶ K. R. A. Ziebeck, P. J. Webster, *J. Phys. Chem. Solids*. **35**, 1, (1974).
- ³⁷ T. Sasaki , T. Kanomata , T. Narita , H. Nishihara , R. Note , H. Yoshida , T. Kaneko, *J. Alloys and Comp.***317**, 406, (2001).

- ³⁸ P. G. van Engen, K. H. J. Buschow, and M. Erman, *J. Magn. Magn. Mater.* **30**, 374 (1983).
- ³⁹ J. Kübler, G. H. Fecher, C. Felser, *Phys. Rev. B* **76**, 024414, (2007).
- ⁴⁰ R. Y. Umetsu, K. Kobayashi, A. Fujita, K. Oikawa, R. Kainuma, K. Ishida, N. Endo, K. Fukamichi, A. Sakuma, *Phys. Rev. B* **72**, 214412, (2005).
- ⁴¹ B. S. D. Ch. S. Varaprasad, A. Rajanikanth, Y. K. Takahashi, K. Hono, *Acta Mater.* **57**, 2702, (2009).
- ⁴² K.H.J. Buschow, P.G. van Engen, *J. Magn. Magn. Mater.* **25**, 90, (1981).
- ⁴³ H. C. Kandpal, G. H. Fecher, C. Felser, *J. Phys. D: Appl. Phys.*, **40**, 1507 (2007).
- ⁴⁴ I. Galanakis, P. H. Dederichs, N. Papanikolaou, *Phys. Rev. B*, **66**, 174429 (2002).
- ⁴⁵ E. Sasioglu, L. M. Sandratskii, P. Bruno, *Phys. Rev. B*, **70**, 024427 (2004) and references therein.
- ⁴⁶ A. Ayuela, J. Enkovaara, K. Ullakko, R. M. Nieminen, *J. Phys. : Cond. Mat.*, **11**, 2017 (1999) and references therein.
- ⁴⁷ A. Chakrabarti, M. Siewert, T. Roy, K. Mondal, A. Banerjee, M. E. Gruner, P. Entel, *Phys. Rev. B*, **88**, 174116 (2013).
- ⁴⁸ J. Worgull, E. Petti, J. Trivisonno, *Phys. Rev. B*, **54**, 15695 (1996).
- ⁴⁹ S. Agduk, G. Gokoglu, *J. Alloys and Comp.* **511**, 9, (2012).
- ⁵⁰ T. Kanomata, Y. Chieda, K. Endo, H. Okada, M. Nagasako, K. Kobayashi, R. Kainuma, R. Y. Umetsu, H. Takahashi, Y. Furutani, H. Nishihara, K. Abe, Y. Miura, M. Shirai, *Phys. Rev. B* **82**, 144415 (2010)
- ⁵¹ T. Roy, D. Pandey and A. Chakrabarti (unpublished).
- ⁵² R. Hill, *Proc. Phys. Soc. A*, **65**, 349 (1952).
- ⁵³ W. Voigt, *Ann. d. Phys. u. Chem. N. F.*, **38**, 573 (1889).
- ⁵⁴ A. Reuss, *Zeit. Angew. Math. Mech. (ZAMM)*, **9**, 49 (1929).
- ⁵⁵ S. F. Pugh, *Phil. Mag.*, **45**, 823 (1954).
- ⁵⁶ H. Niu, X. Q. Chen, P. Liu, W. Xing, X. Cheng, D. Li, Y. Li, *Scientific Reports*, **2**, 718 (2012).
- ⁵⁷ C. -M. Li, H. -B. Luo, Q. -M. Hu, R. Yang, B. Johansson, L. Vitos, *Phys. Rev. B*, **84**, 024206 (2011).
- ⁵⁸ P. J. Brown, A. Y. Bargawi, J. Crangle, K. -U. Neumann, K. R. A. Ziebeck, *J. Phys.: Cond. Mat.*, **11**, 4715 (1999).
- ⁵⁹ J. C. Suits, *Solid State Comm.*, **18**, 423 (1976).
- ⁶⁰ R. Arroyave, A. Junkaew, A. Chivukula, S. Bajaj, C.-Y. Yao, A. Garay, *Acta Mater.*, **58**, 5220 (2010).

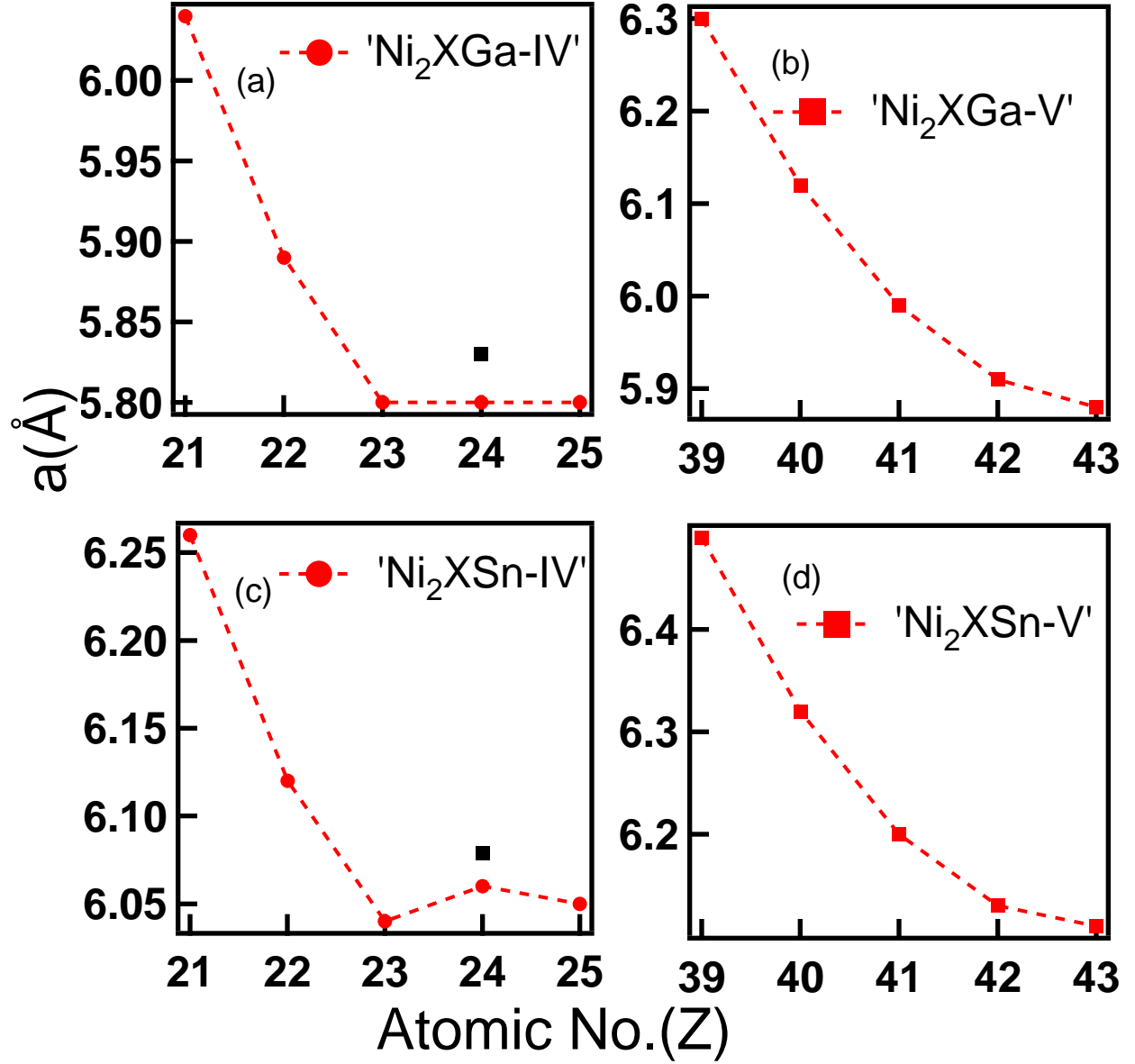


FIG. 1: Variation of lattice parameter as a function of Z of B elements for Ni_2BC alloy ($C = Ga, Sn$); $X=B$ atoms being first five transition metal elements of period IV (left panel) and V (right panel).

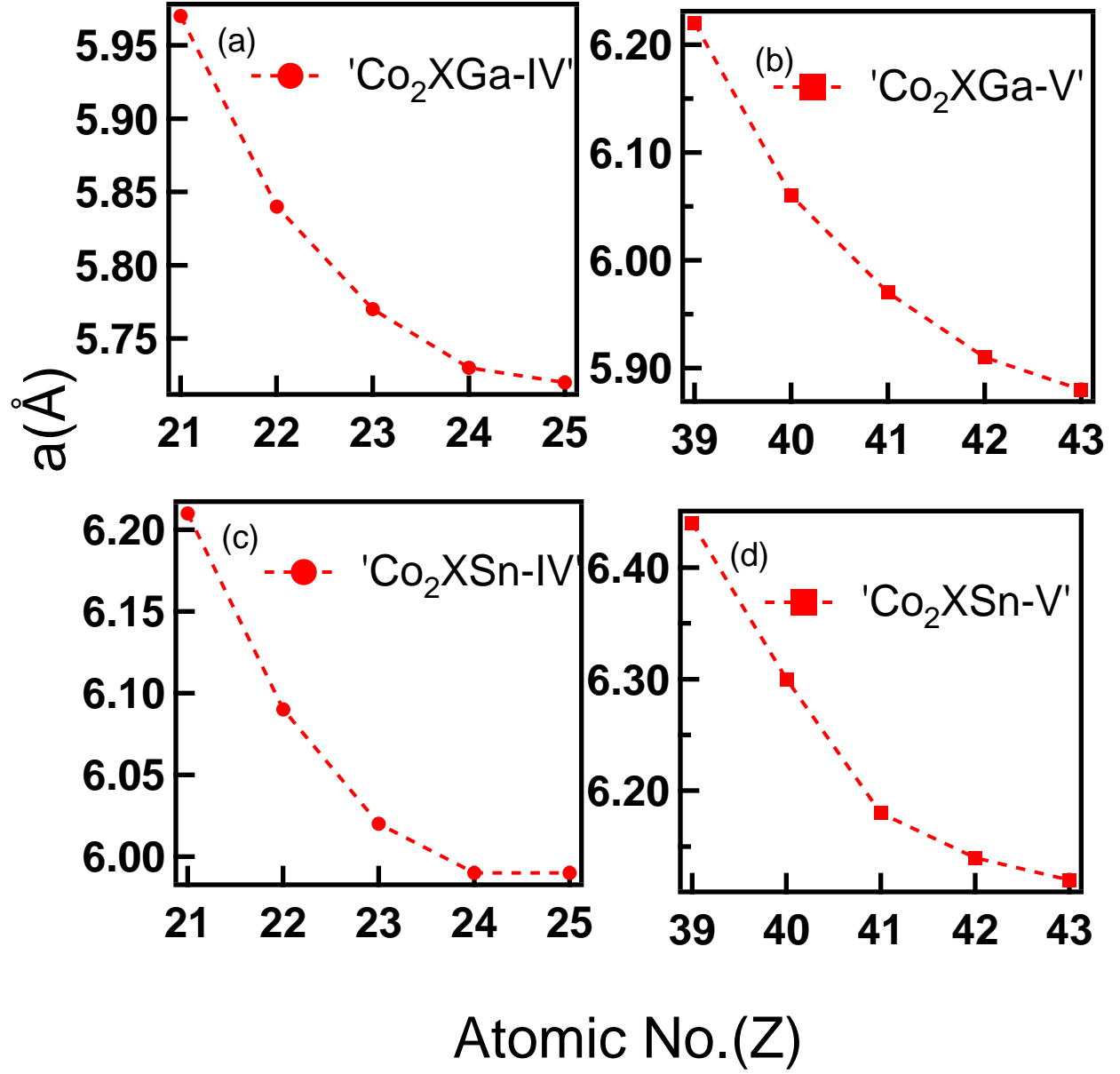


FIG. 2: Variation of lattice parameter as a function of Z of B elements for Co_2BC alloy ($C = \text{Ga, Sn}$); $\text{X}=\text{B}$ atoms being first five transition metal elements of period IV (left panel) and V (right panel).

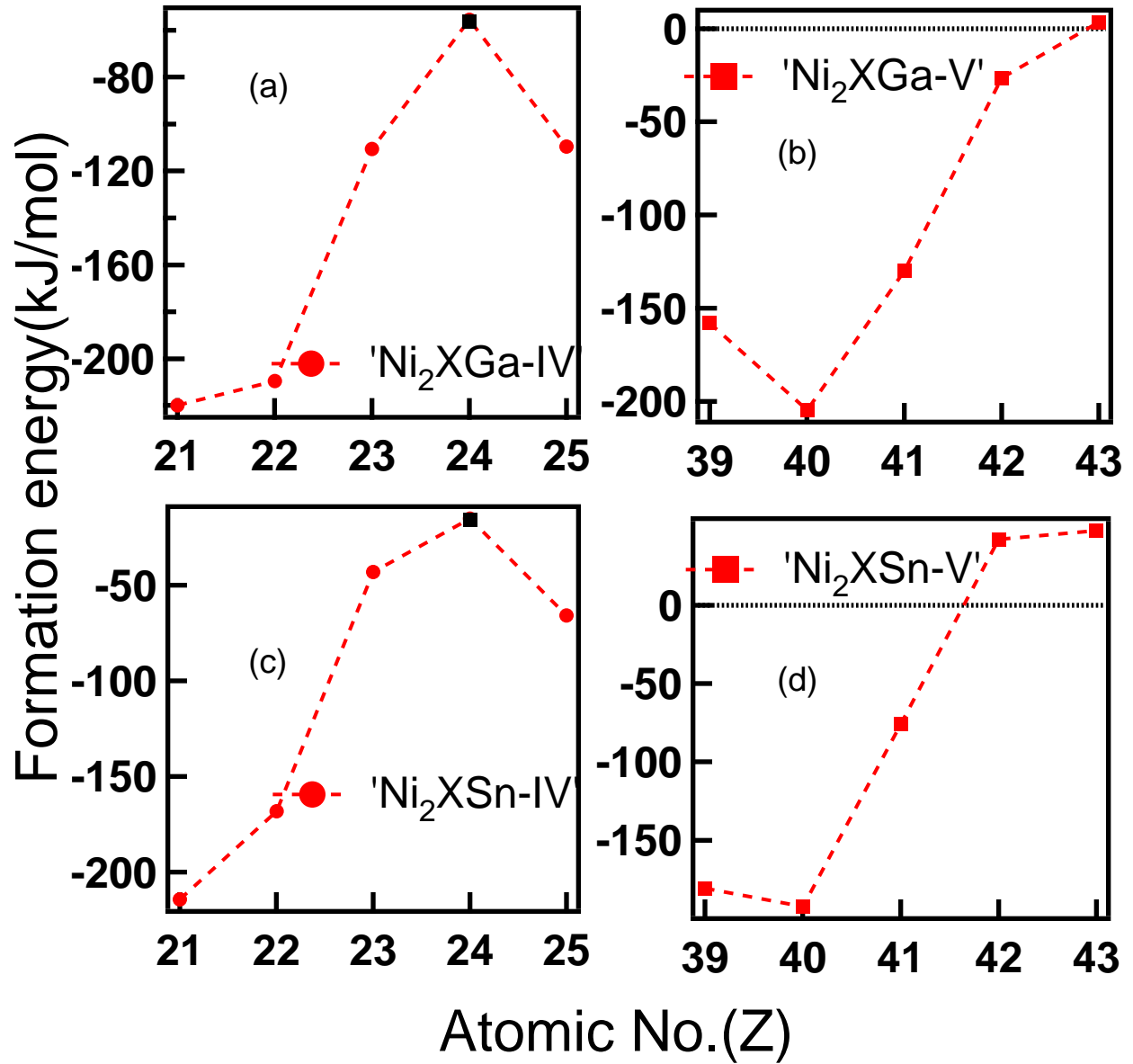


FIG. 3: Variation of formation energy as a function of Z of B elements for Ni_2BC alloy ($C = Ga, Sn$); $X=B$ atoms being first five transition metal elements of period IV (left panel) and V (right panel).

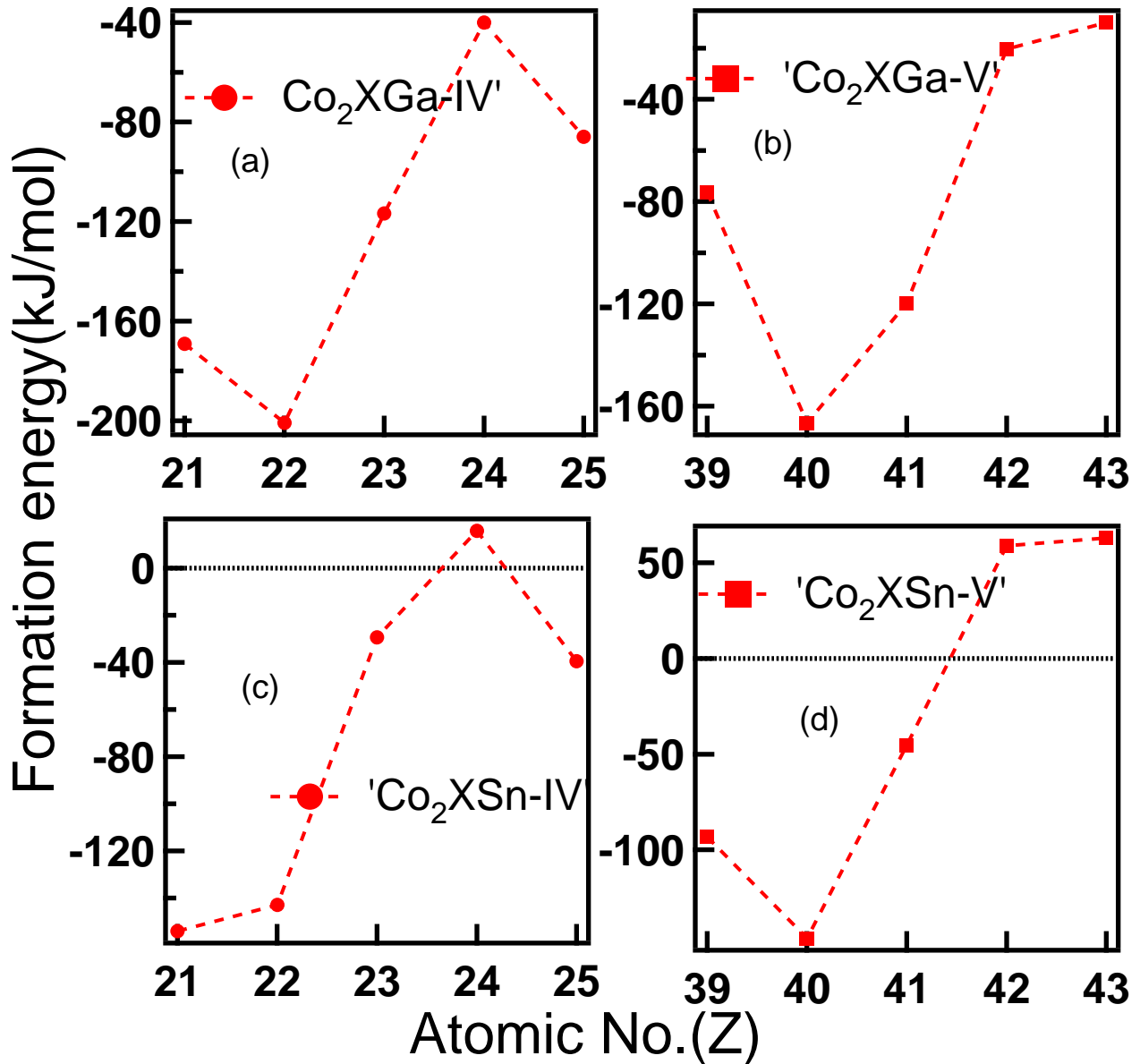


FIG. 4: Variation of formation energy as a function of Z of B elements for Co_2BC alloy ($C = \text{Ga, Sn}$); $X=B$ atoms being first five transition metal elements of period IV (left panel) and V (right panel).

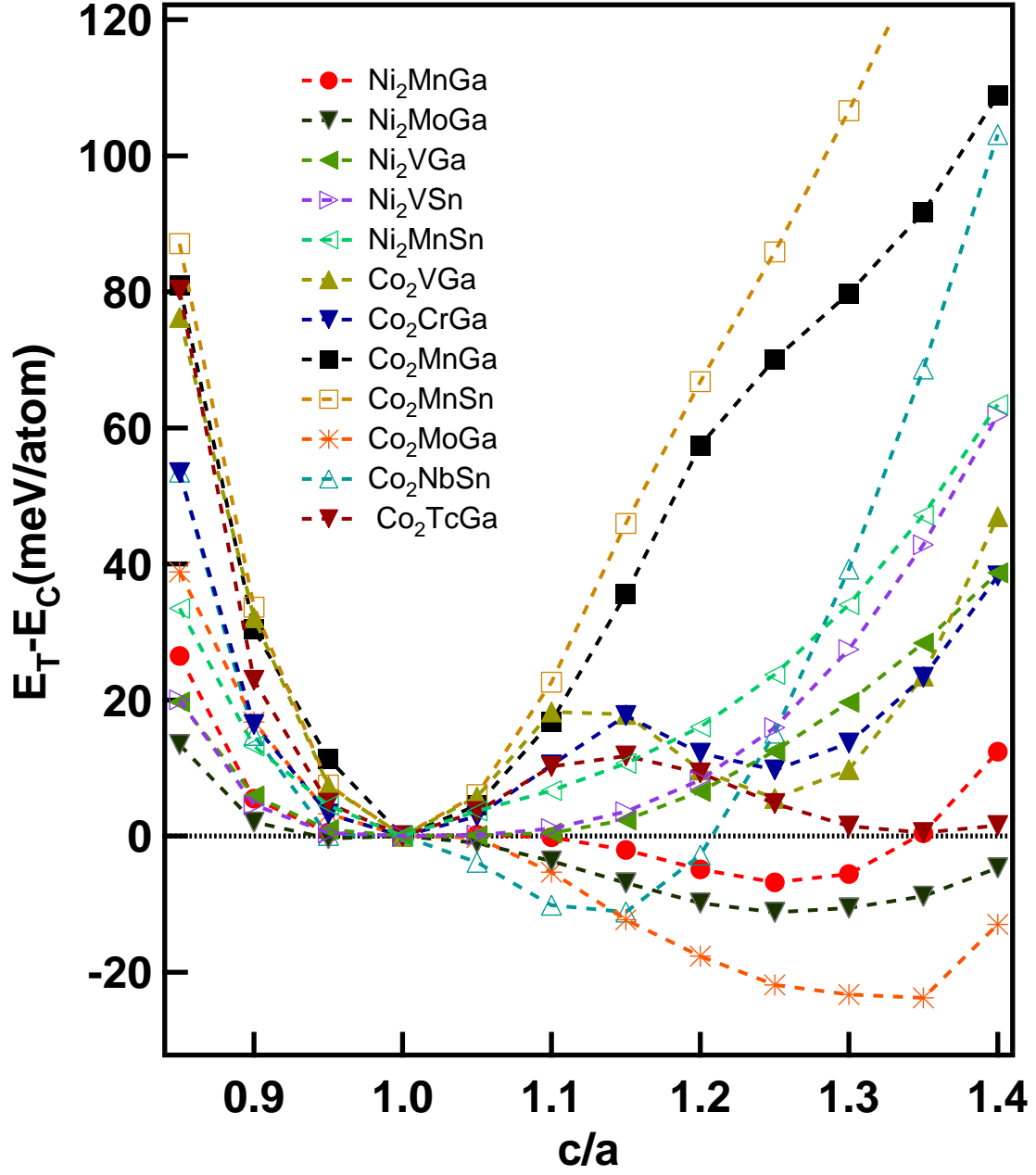


FIG. 5: Energy difference between the crystal structures with tetragonal (T) and cubic (C) symmetries, of some typical materials represented as $E_T - E_C$ (in units of meV per atom), as a function of the ratio of lattice constants c and a . The energies have been normalized with respect to the energy of the respective cubic austenite phase of each material.

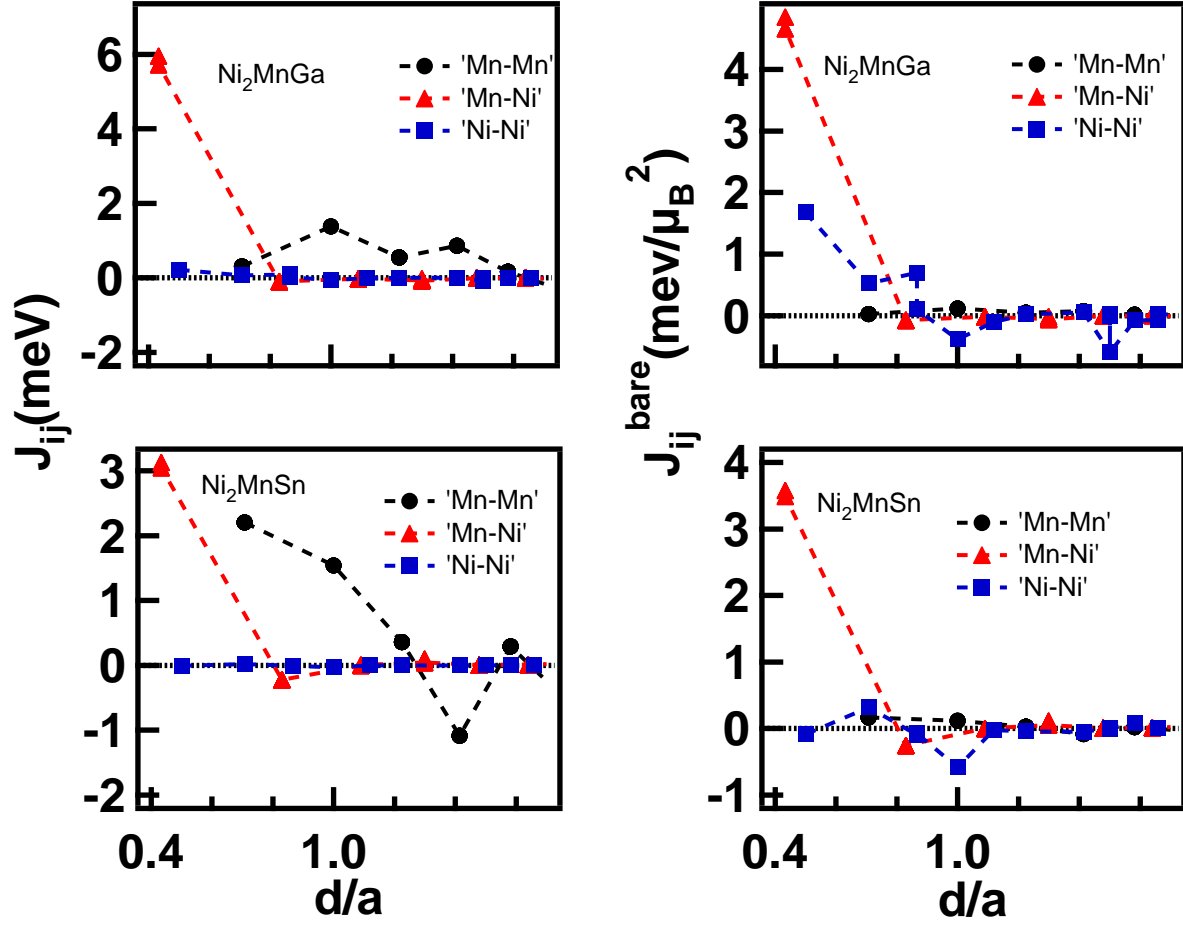


FIG. 6: J_{ij} parameters between different atoms of Ni_2MnGa and Ni_2MnSn as a function of distance between the atoms i and j (normalized with respect to the respective lattice constant).

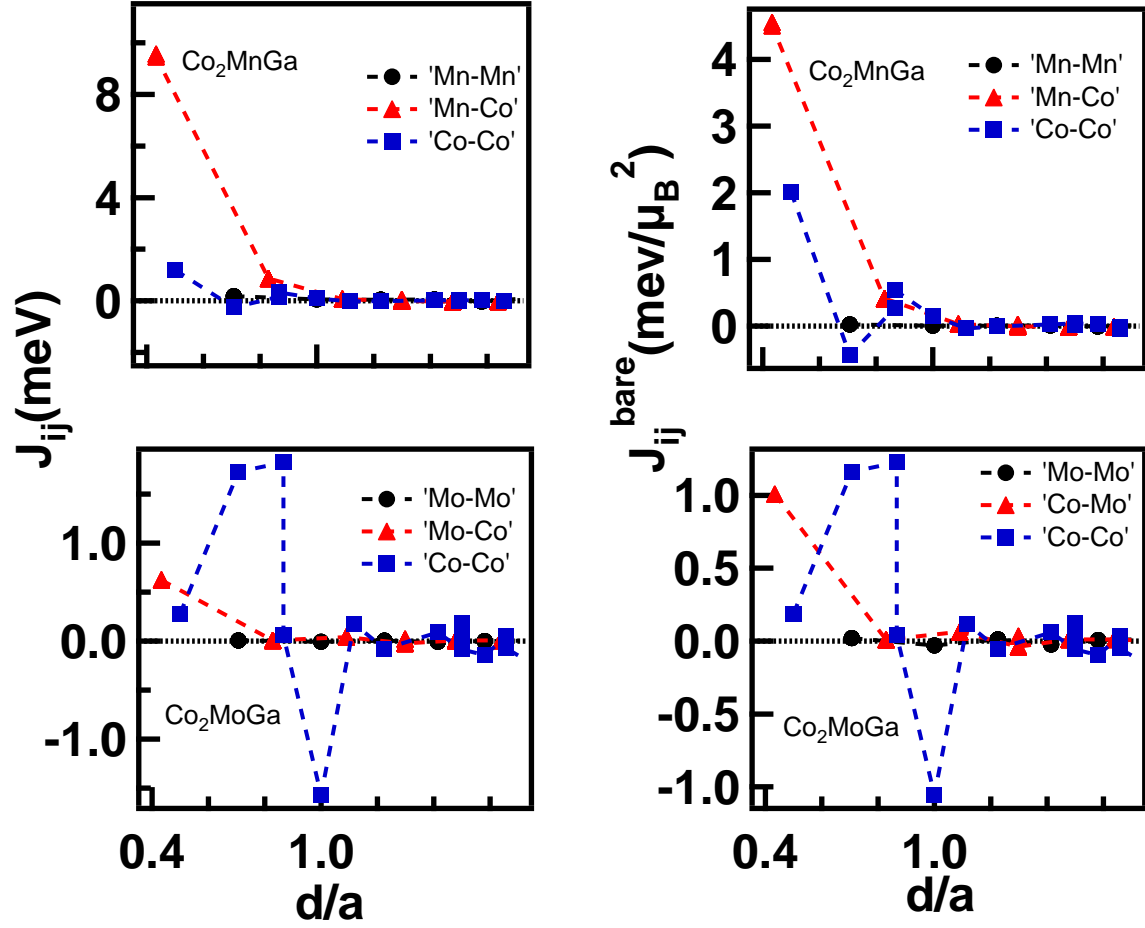


FIG. 7: J_{ij} parameters between different atoms of Co_2MnGa and Co_2MoGa as a function of distance between the atoms i and j (normalized with respect to the respective lattice constant).

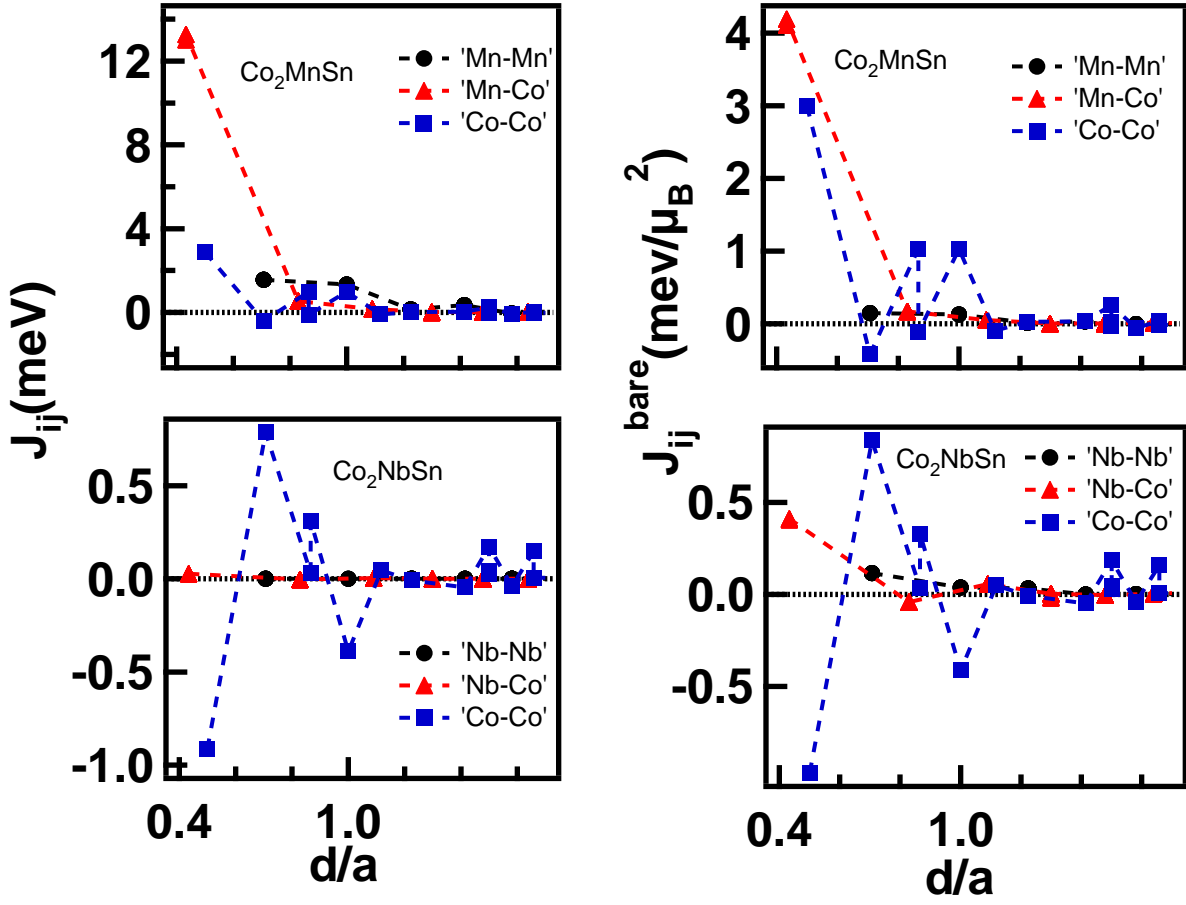


FIG. 8: J_{ij} parameters between different atoms of Co_2MnSn and Co_2NbSn as a function of distance between the atoms i and j (normalized with respect to the respective lattice constant).

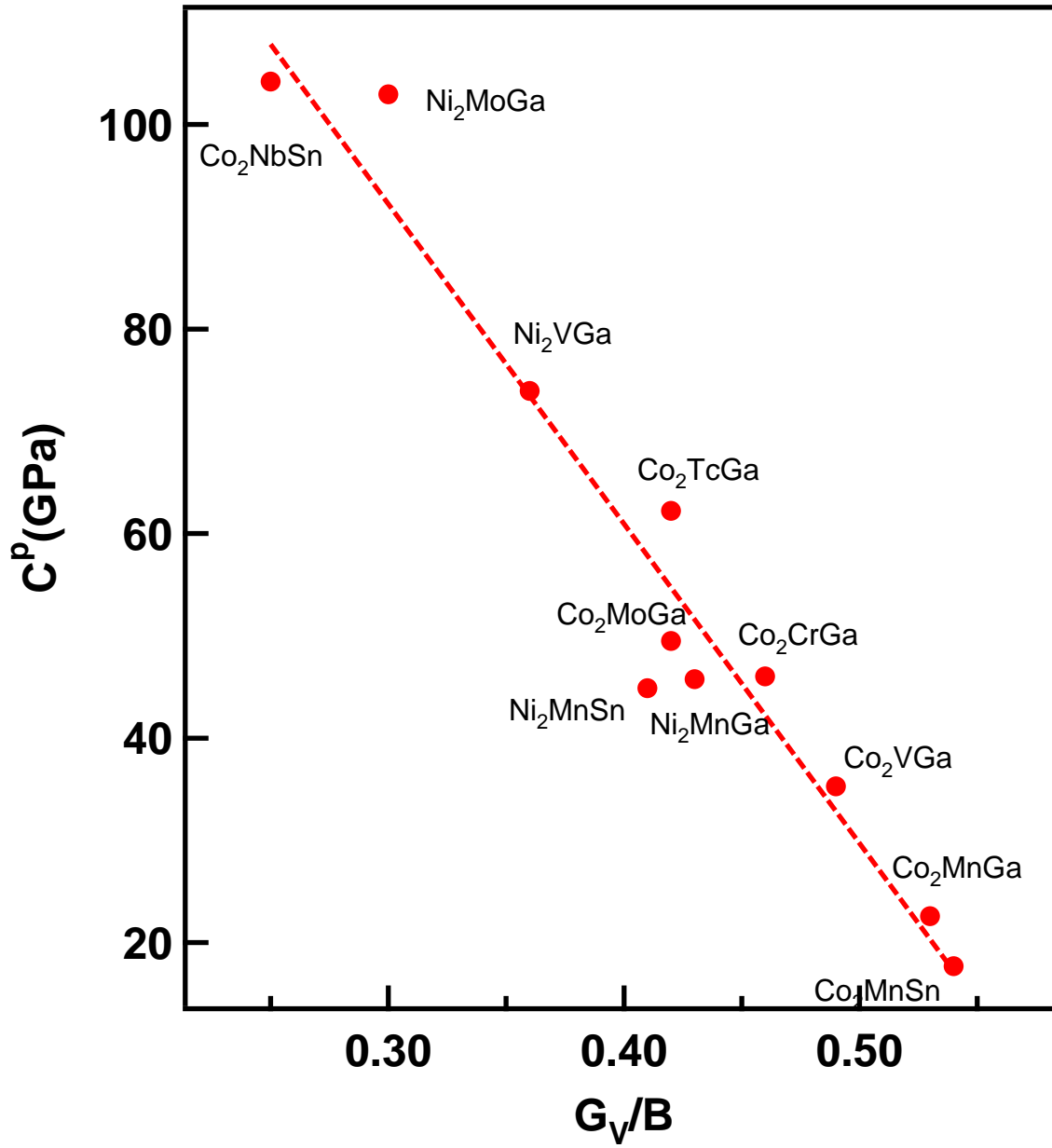


FIG. 9: Cauchy pressure, C^P , versus G_V/B ; a linear fitting of all the data is carried out and shown here. An inverse linear-type relation is seen to exist between the two parameters (see text).

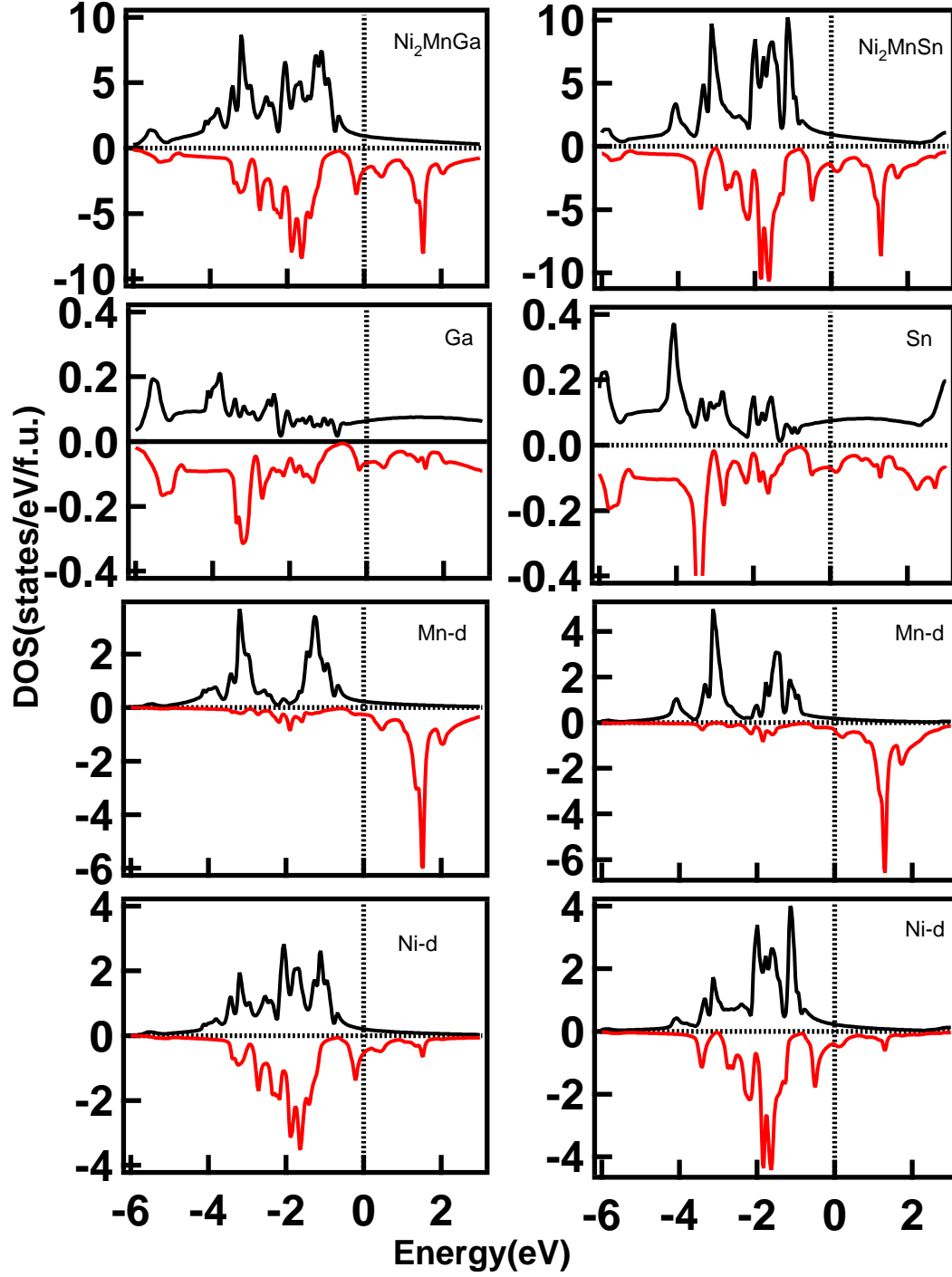


FIG. 10: The left and right set of panels depict the density of states of Ni_2MnGa and Ni_2MnSn materials, respectively. From top to bottom panel, first the total density of states as a function of energy has been plotted. Next panel shows the partial density of states of the Ni atom. Partial density of states of the Mn atom and the C atom are shown in the third and the fourth panels. The DOS of the C atom is multiplied by a factor of 10. The Fermi level is at 0 eV.

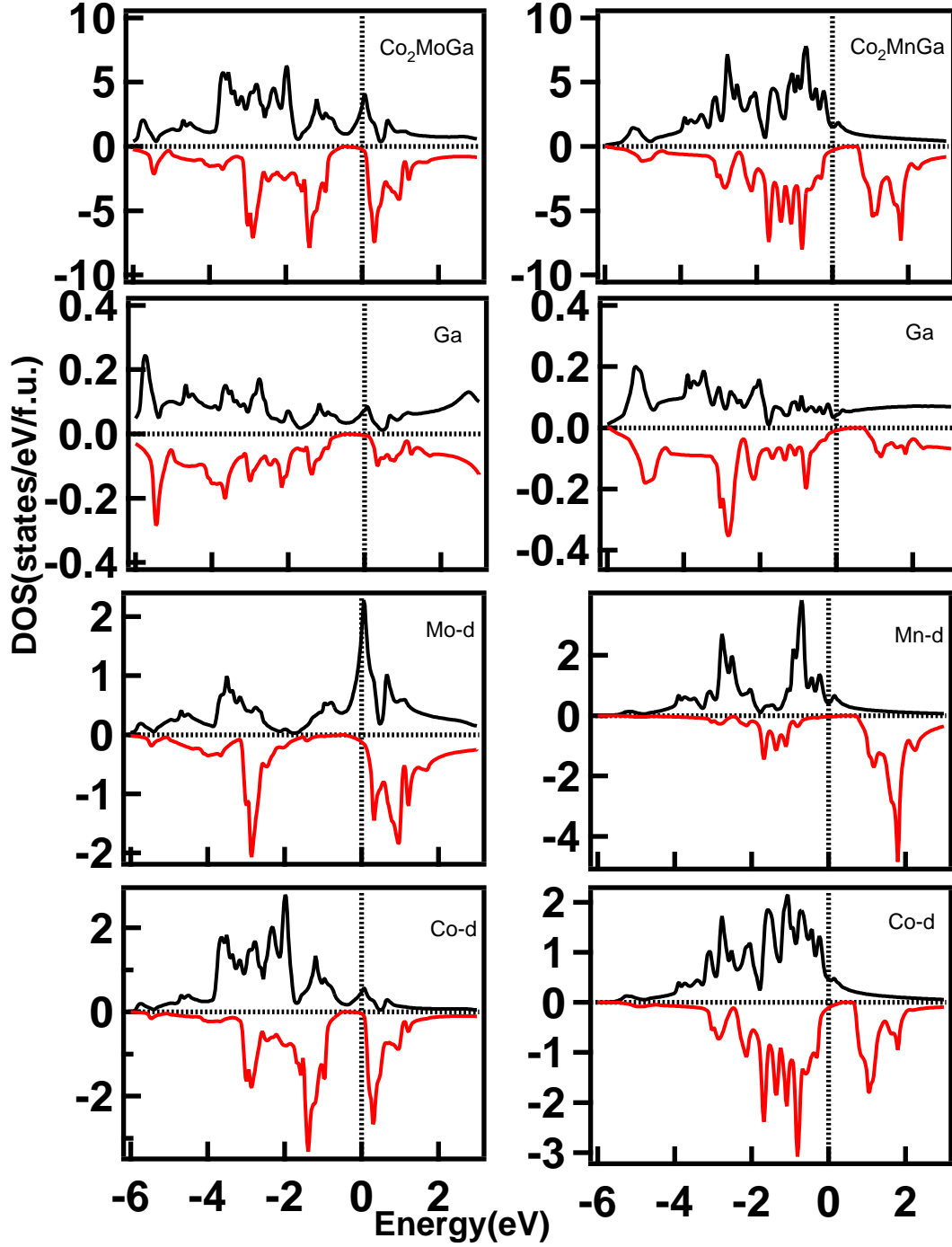


FIG. 11: The left and right set of panels depict the density of states of Co_2MoGa and Co_2MnGa materials, respectively. From top to bottom panel: first the total density of states as a function of energy has been plotted. Next panel shows the partial density of states of the Co atom. Partial density of states of the B atom and the Ga atom are shown in the third and the fourth panels. The DOS of the C atom is multiplied by a factor of 10. The Fermi level is at 0 eV.

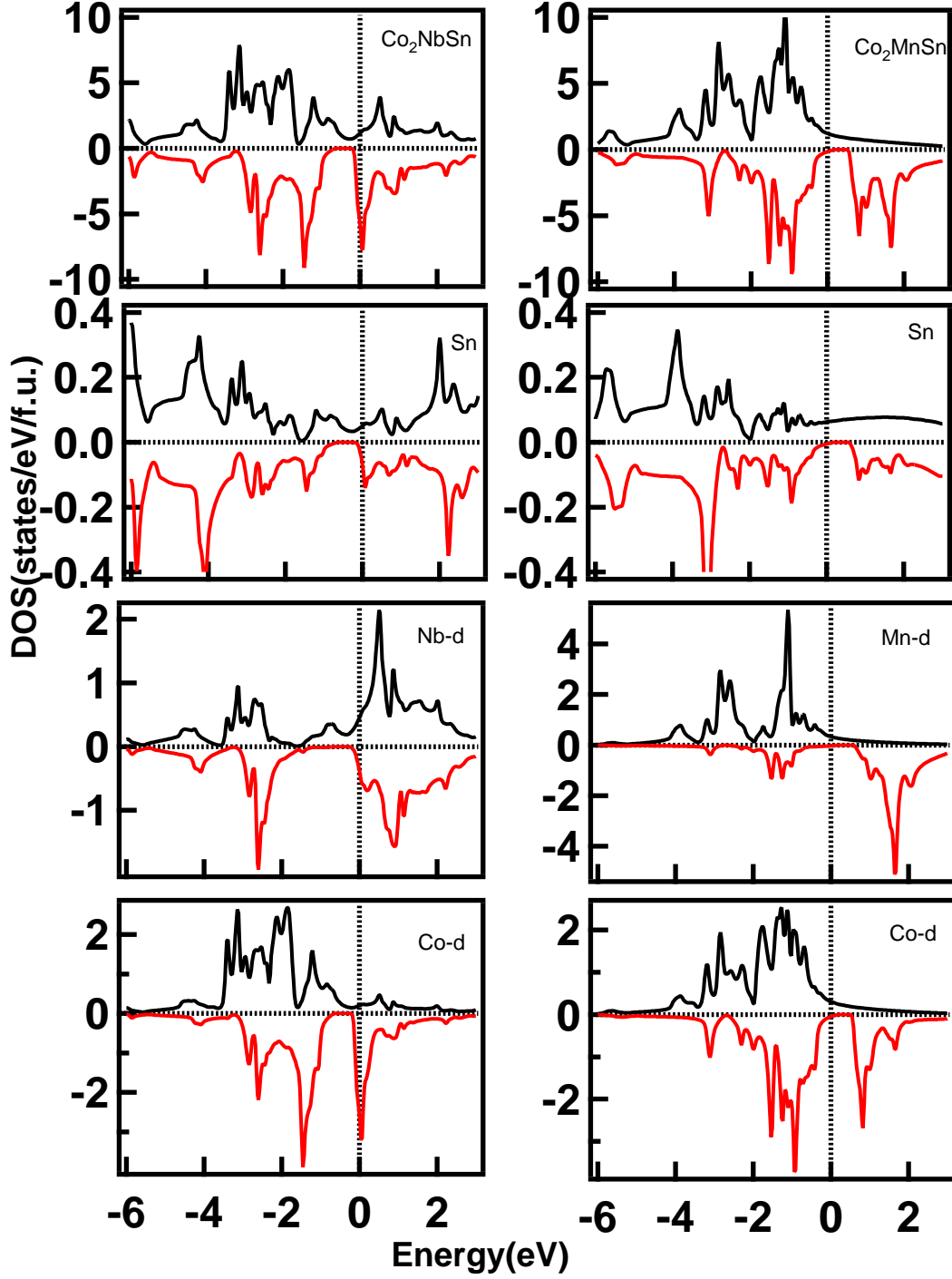


FIG. 12: The left and right set of panels depict the density of states of Co_2NbSn and Co_2MnSn materials, respectively. From top to bottom panel: first the total density of states as a function of energy has been plotted. Next panel shows the partial density of states of the Co atom. Partial density of states of the B atom and the Sn atom are shown in the third and the fourth panels. The DOS of the C atom is multiplied by a factor of 10. The Fermi level is at 0 eV.

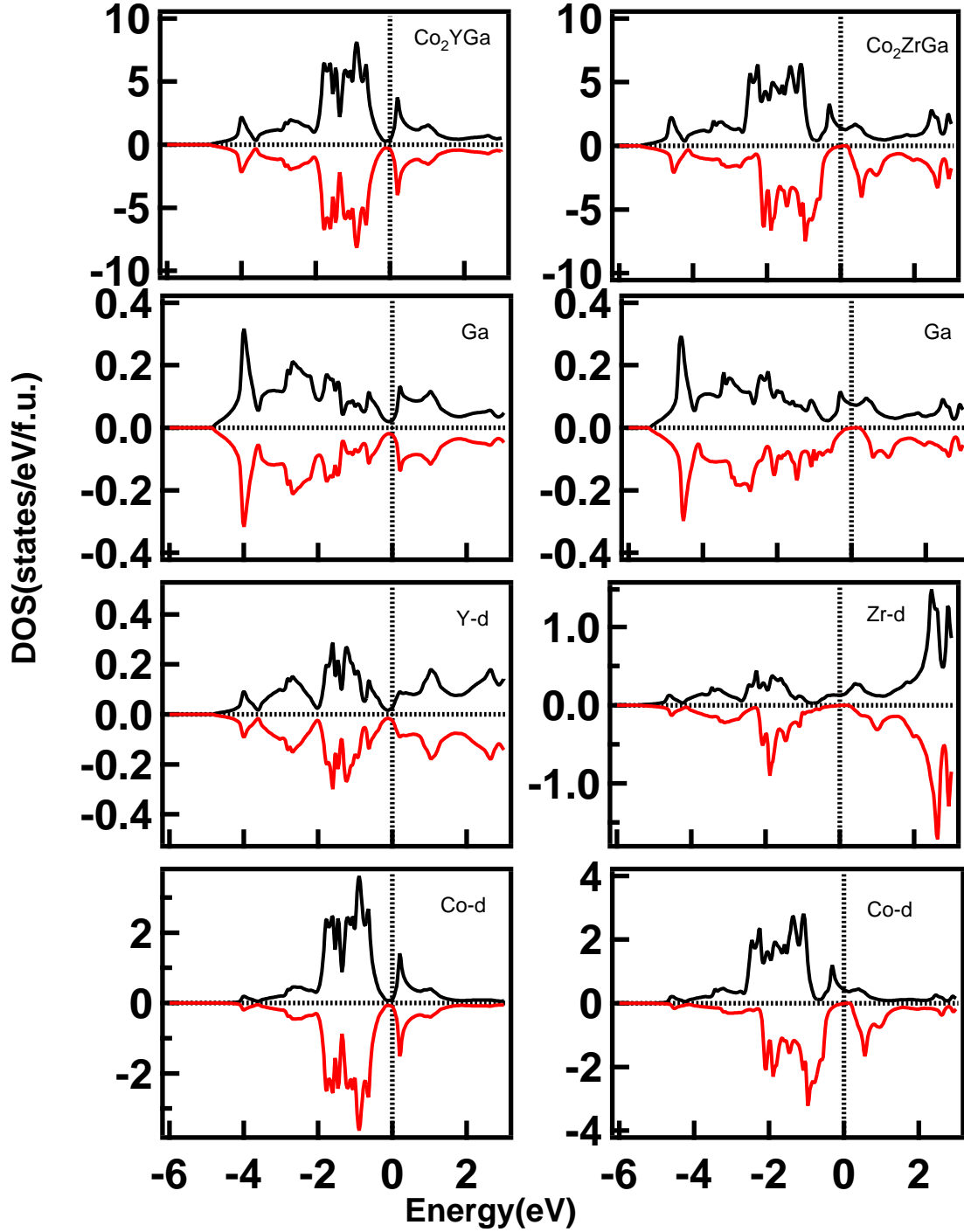


FIG. 13: The left and right set of panels depict the density of states of Co_2YGa and Co_2ZrGa materials, respectively. From top to bottom panel: first the total density of states as a function of energy has been plotted. Next panel shows the partial density of states of the Co atom. Partial density of states of the *B* atom and the Ga atom are shown in the third and the fourth panels. The DOS of the *C* atom is multiplied by a factor of 10. The Fermi level is at 0 eV.

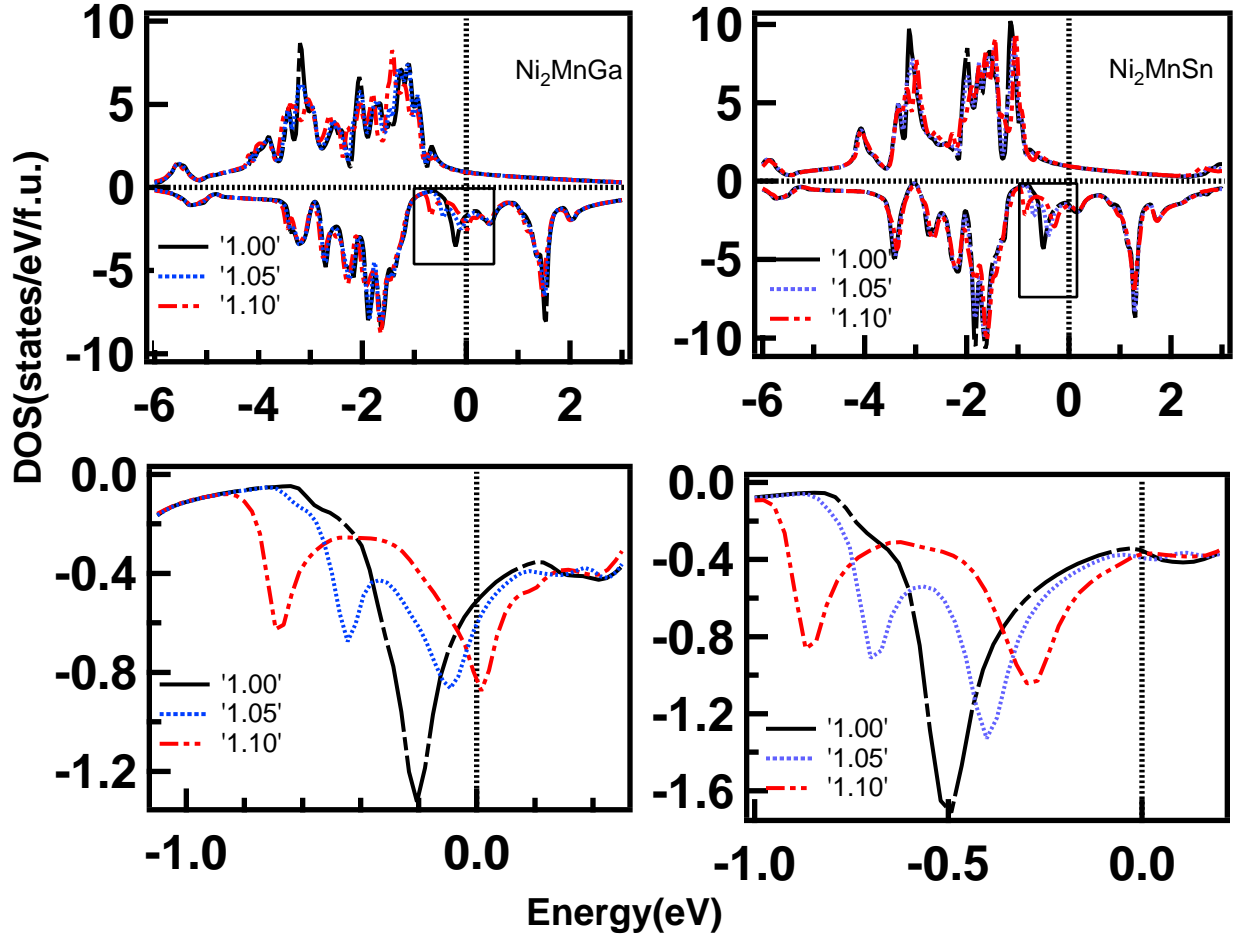


FIG. 14: The density of states as a function of energy has been plotted for the cubic and tetragonal phases, with c/a varying from 1 to 1.10 in steps of 0.05 for materials Ni_2MnGa and Ni_2MnSn in left and right panels, respectively. Panels below show the down spin density near the Fermi level in an expanded scale for respective materials. The Fermi level is at 0 eV.

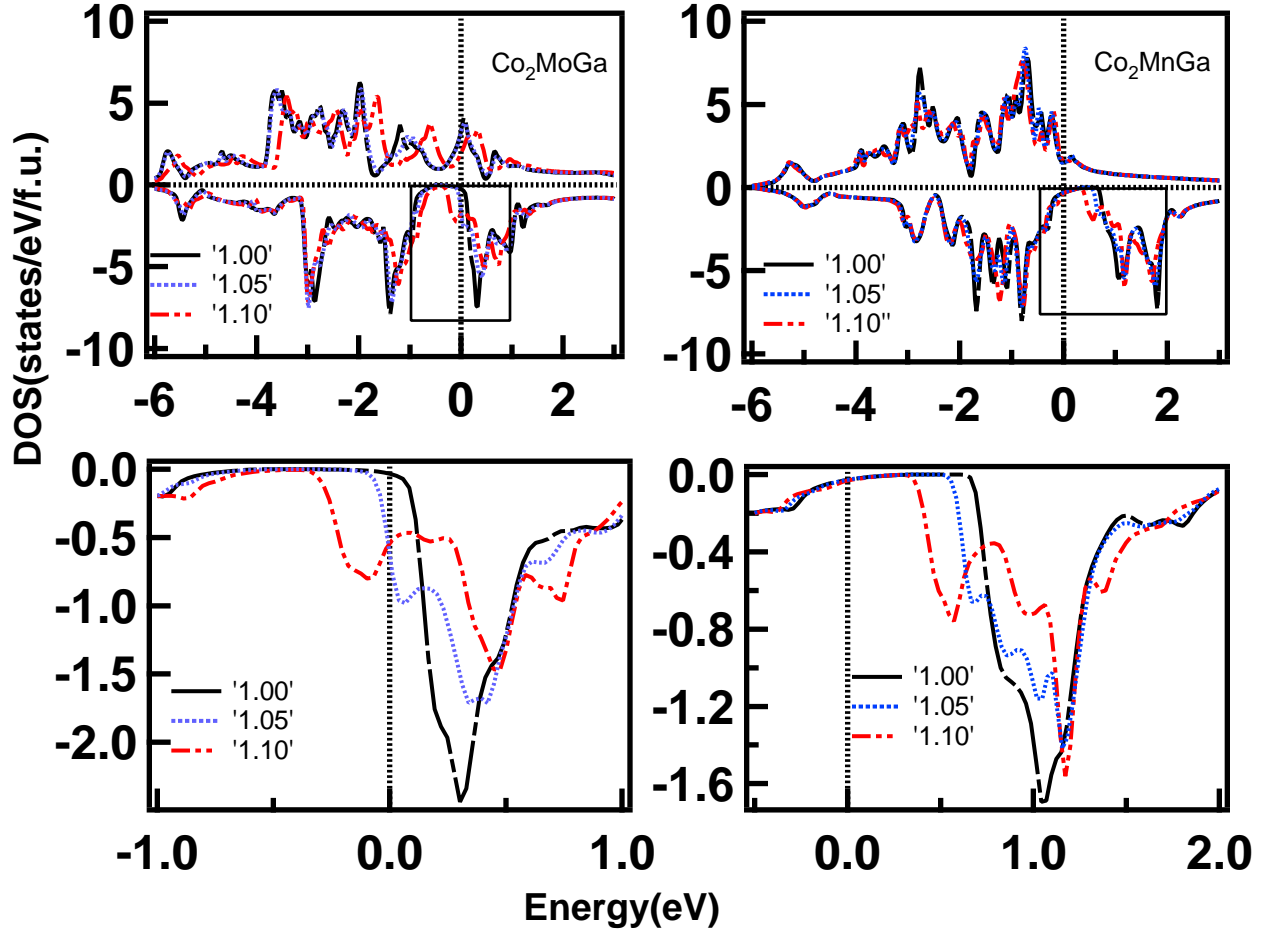


FIG. 15: The density of states as a function of energy has been plotted for the cubic and tetragonal phases, with c/a varying from 1 to 1.10 in steps of 0.05 for materials Co_2MoGa and Co_2MnGa in left and right panels, respectively. Panels below show the down spin density near the Fermi level in an expanded scale for respective materials. The Fermi level is at 0 eV.

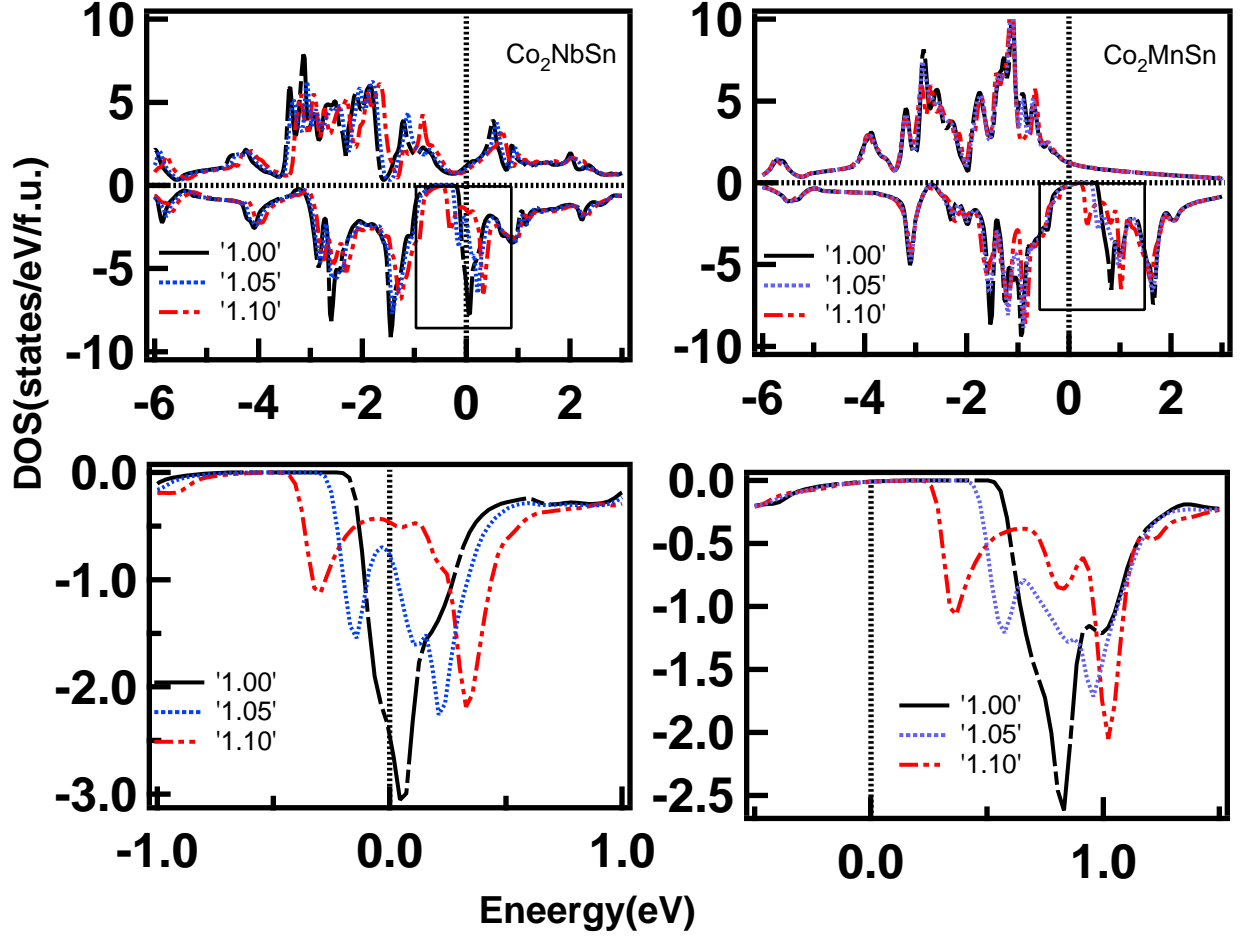


FIG. 16: The density of states as a function of energy has been plotted for the cubic and tetragonal phases, with c/a varying from 1 to 1.10 in steps of 0.05 for materials Co_2NbSn and Co_2MnSn in left and right panels, respectively. Panels below show the down spin density near the Fermi level in an expanded scale for respective materials. The Fermi level is at 0 eV.

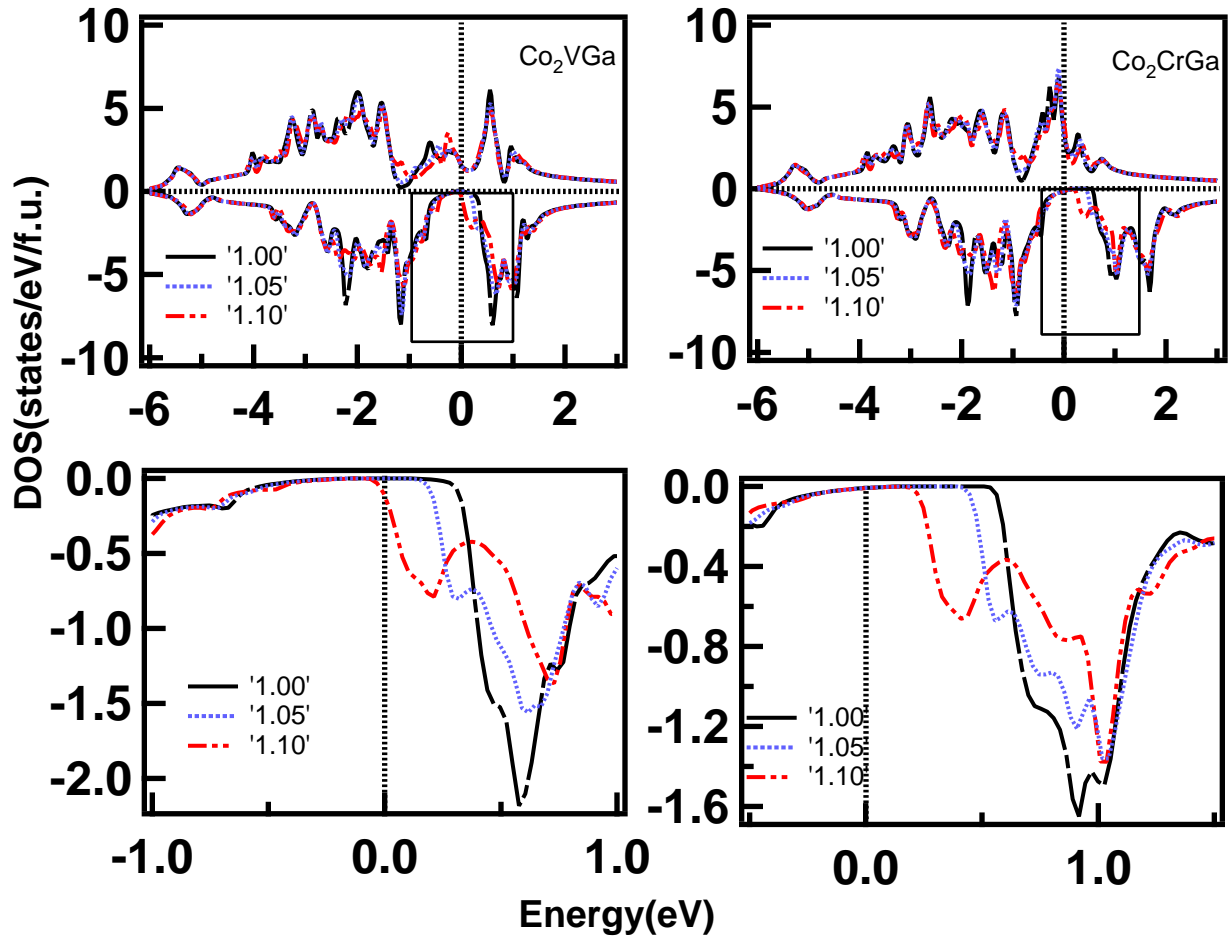


FIG. 17: The density of states as a function of energy has been plotted for the cubic and tetragonal phases, with c/a varying from 1 to 1.10 in steps of 0.05 for materials Co_2VGa and Co_2CrGa in left and right panels, respectively. Panels below show the down spin density near the Fermi level in an expanded scale for respective materials. The Fermi level is at 0 eV.